

# Homophily Within and Across Groups

Abbas K. Rizi,<sup>1,2,3</sup> Riccardo Michielan,<sup>4</sup> Clara Stegehuis,<sup>4</sup> and Mikko Kivela<sup>3</sup>

<sup>1</sup>*DTU Compute, Technical University of Denmark, Kongens Lyngby 2800, Denmark*

<sup>2</sup>*Copenhagen Center for Social Data Science, University of Copenhagen, Denmark*

<sup>3</sup>*Department of Computer Science, School of Science, Aalto University, FI-00076, Finland*

<sup>4</sup>*Faculty of Electrical Engineering, Mathematics and Computer Science, University of Twente, Enschede, Netherlands*

(Dated: December 12, 2024)

Traditional social network analysis often models homophily—the tendency of similar individuals to form connections—using a single parameter, overlooking finer biases within and across groups. We present an exponential family model that integrates both local and global homophily, distinguishing between strong homophily within tightly knit cliques and weak homophily spanning broader community interactions. By modeling these forms of homophily through a maximum entropy approach and deriving the network behavior under percolation, we show how higher-order assortative mixing influences network dynamics. Our framework is useful for decomposing homophily into finer levels and studying the spread of information and diseases, influence dynamics, and innovation diffusion. We demonstrate that the interaction between different levels of homophily results in complex percolation thresholds. We tested our model on various datasets with distinct homophily patterns, showcasing its applicability. These homophilic connections significantly affect the effectiveness of intervention and mitigation strategies. Hence, our findings have important implications for improving public health measures, understanding information dissemination on social media, and optimizing intervention strategies.

## I. INTRODUCTION

Human interactions naturally lead to forming communities and groups, often characterized by connections between individuals with similar attributes—a phenomenon known as assortativity or homophily [1, 2]. This principle, where “birds of a feather flock together,” affects not only friendship formation but also social selection, peer influence, organizational behavior, and online interactions—shaping the overall resilience and dynamism of social networks [2–4]. Engagement patterns on platforms like Facebook and X suggest that, while individuals tend to initially connect with similar others, they often end up interacting more intensively with people holding opposing views during public discussions and debates, particularly on polarizing topics [5–7]. This gives rise to a dual-layer homophily: local homophily that guides connection formation and global homophily that emerges from interactions across broader, more diverse viewpoints. These layers manifest similarly in contexts like interdisciplinary citation networks, where researchers engage within their fields while also citing work across disciplines [8], or in global trade networks, where countries exchange diverse goods beyond their primary economic alliances [9].

In social networks, the strength of interpersonal ties between individuals plays a crucial role in shaping interaction dynamics [10, 11]. Strong bonds, characterized by frequent and emotionally significant exchanges, are vital for social support and the transmission of complex information, particularly among close friends and family members [10]. Groups foster cohesion and influence the broader integration of social networks by modulating the formation and role of strong ties [12, 13]. In contrast, weak bonds, such as those between acquaintances, are instrumental in spreading information across

different social circles and promoting the diffusion of new ideas [14]. Moreover, weak ties are key in spreading contagions, as they bridge disparate communities, facilitating the transmission of infections across network boundaries [15–17]. Bond strength and homophily mutually influence each other during network evolution [18]. For instance, strong ties are often formed based on race in diverse environments [14, 19], whereas weak ties exhibit gender homophily [20]. This distinction between strong and weak ties highlights their influence on network resilience and spreading dynamics. Strong ties can increase the epidemic threshold, acting as barriers to rapid contagion spread, while weak ties are crucial for bridging social groups and accelerating innovation diffusion [10, 21].

Homophily in social network analysis is often represented as a network-wide property controlling or emerging from dyadic interactions. Such approaches often overlook the nuanced effects of strong (local) and weak (global) homophilic interactions on group dynamics. While generating a network given a degree sequence and a homophily value is relatively straightforward [22, 23], creating random graphs with finer details—such as differentiated biases in connections across groups—remains beyond the capabilities of existing models. Incorporating homophily in the context of group structures introduces significant challenges, yet it enables the representation of varying homophilic tendencies within different groups and facilitates the integration of multiple layers of interaction [24]. Moreover, homophily is inherently multi-dimensional, arising from attributes such as race, gender, or shared interests. Capturing these diverse factors within network models is, however, computationally demanding, especially when attempting to account for all potential homophilic connections, which makes comprehensive modeling practically infeasible [25].

In this paper, we propose a comprehensive framework that decomposes the dyadic homophily across groups and inside groups of different sizes, aligning naturally with well-established theories in social science. We provide a detailed understanding of the effects of these different types of homophiles on the connectivity of the networks, which has implications for spreading phenomena. We show that a maximum entropy approach that only fits one parameter per group size is able to capture the homophily levels in several network data sets remarkably well. While it is possible to introduce a simplicial homophily score to capture higher-order homophily within simplicial complexes—providing metrics for group-level homophily beyond dyadic connections [26]—our approach takes a simpler and more flexible route. Furthermore, these data show that homophily patterns within different group sizes may be quite different, sometimes increasing in group sizes and sometimes decreasing in group sizes. We show that these different homophily levels can have a crucial impact on network spreading processes and percolation: when percolation levels are different within and between groups, in some cases different homophily levels may increase the percolation threshold, while in other cases, the homophily levels decrease the percolation threshold.

The paper is structured as follows: In Section II, we present the proposed network model, describing its statistical properties and group interactions. In Section III, we show how this model can describe many different datasets and it enables us to define local homophily consistently across groups of any size. In Section IV, we investigate the implications of these models for percolation processes and analyze their impact on connectivity and epidemic thresholds. We leave some less crucial details to the appendix.

## II. MODEL DESCRIPTION

A social network can be represented as a collection of nodes connected by various relationships and interactions. We will create a simple undirected graph  $G$  that consists of different  $c$ -clique-graphs  $G_c$ . The  $N$  nodes of  $G$  are divided into  $N_r$  red nodes and  $N_b = N - N_r$  blue nodes, with possible red-red, red-blue, or blue-blue links.

We now describe how each clique graph  $G_c$  is generated. First, as the nodes of  $G_c$  have two possible colors, each  $c$ -clique can be classified into one of the  $c + 1$  types, depending on its number of red nodes. For example, Fig. 1a illustrates four possible configurations of a 3-clique with 0, 1, 2, or 3 red nodes. We denote the distribution of these clique types by the vector  $\mathbf{F}_c$ , where  $F_{c,i}$  represents the proportion of  $c$ -cliques with  $i$  red nodes. This vector provides insights into the local homophily of the graph. For example, when  $c = 3$ , higher values of  $F_{3,0}$  and  $F_{3,3}$  relative to  $F_{3,1}$  and  $F_{3,2}$  indicate stronger local homophily, as cliques composed entirely of nodes of the same color (all red or all blue) represent maximum

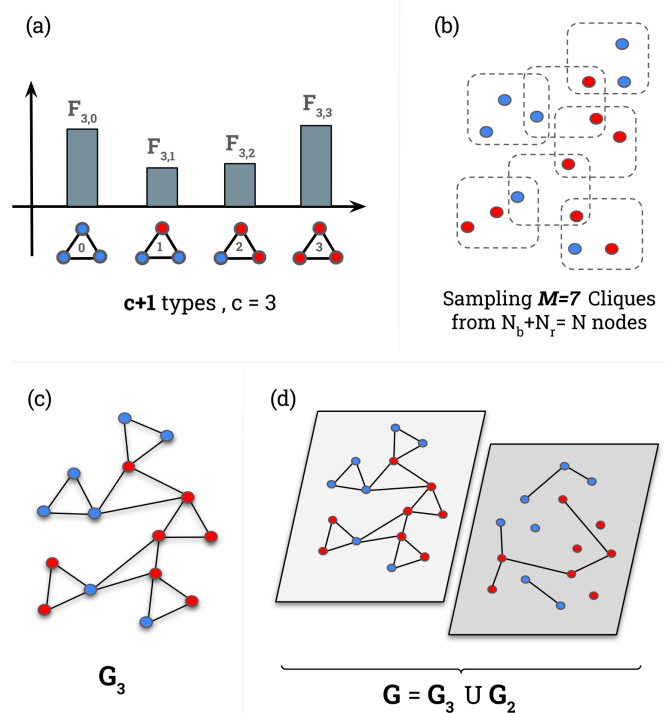


FIG. 1. Creating a homophilic clique network with eight red and six blue nodes. (a) With two colors, there can be  $c + 1$  types of  $c$ -cliques distributed according to  $\mathbf{F}_c$ . Here  $c = 3$ . (b)  $M_3 = 7$  cliques are sampled with replacement from the available colored nodes. Consequently, the relative frequency  $F_{c,i}$ , where  $i$  represents the number of red nodes in each clique, and the abundance of red nodes can influence the degree heterogeneity of red nodes. (c)  $G_3$  is built by sampling seven 3-cliques. (d) Final network  $G = G_3 \cup G_2$  shapes after merging different clique layers where they share the same nodes. Here  $G_2$  is built through a similar procedure with a different  $M_2$  and  $\mathbf{F}_2$ . In general, a network can be made of the union of many different layer-graphs  $G = \bigcup G_c$ .

homophily at the local level.

We then sample  $M_c$  cliques of size  $c$ , whose types are sampled according to the distribution  $\mathbf{F}_c$ . A clique of type  $i$  is sampled by sampling  $i$  uniformly chosen red vertices, and  $c - i$  uniformly chosen blue vertices. This means that a single node can belong to multiple cliques.

Homophily is a measure of the tendency of nodes to connect to similar others. The homophily of each clique type can be computed using the standard Coleman Homophily index [27, 28]. This index is calculated as the normalized difference between the number of intra-group connections in the network and its expected value if the links were uniformly placed randomly in the network. If  $e_{rr}$ ,  $e_{bb}$ , and  $e_{rb}$  are the link densities between colored nodes, and respectively  $n_r = N_r/N$  and  $n_b = 1 - n_r$  are the density of red and blue nodes, the Coleman homophily index  $h$  of the network is defined as

$$h = \frac{e_{rr} + e_{bb} - n_r^2 - n_b^2}{1 - n_r^2 - n_b^2}. \quad (1)$$

In our case, each clique type contributes differently to the total homophily of the network  $G_c$ . The contribution of links within a clique of size  $c$  and type  $i$ , i.e., containing  $i$  red nodes, to the homophily index is

$$h_{c,i} = \frac{\frac{\binom{i}{2} + \binom{c-i}{2}}{\binom{c}{2}} - n_r^2 - n_b^2}{1 - n_r^2 - n_b^2}. \quad (2)$$

The choices  $i = 0$  and  $i = c$ , cliques with all red or blue nodes, yield the intrinsic homophily,  $h_{c,i}$  equal to 1. On the other hand, the most heterophilic configuration is achieved when the numerator in Eq. (2) is the smallest possible. This happens when, depending on the parity of  $c$ ,  $i = \frac{c}{2}$  or  $i = \frac{c \pm 1}{2}$ , that is, for the most heterogeneously colored clique types. In particular, we have

$$h_{c,c/2} = \frac{\frac{c-2}{2c-2} - n_r^2 - n_b^2}{1 - n_r^2 - n_b^2}, \quad (3)$$

and

$$h_{c,(c \pm 1)/2} = \frac{\frac{c-1}{2c} - n_r^2 - n_b^2}{1 - n_r^2 - n_b^2}. \quad (4)$$

The homophily value of a network layer  $G_c$  is then obtained as the weighted average of the homophily contributions of all different clique types of size  $c$ , yielding

$$h_c = \sum_i h_{c,i} F_{c,i} \quad (5)$$

All the layers have the same red and blue nodes and therefore for any  $c$ ,

$$N_{c,r} = N_r = \frac{1}{c} \sum_i i F_{c,i}. \quad (6)$$

These equations allow us to calculate the homophily index  $h_c$  for every clique size  $c$ , providing insight into the level of homophily within different group sizes.

### A. Maximum Entropy Distribution for Local Homophilies

As the clique-homophily level  $h_c$  of Eq. (5) is an average over all possible distributions of a  $c$ -clique into red and blue nodes, this means that there are many different choices of the  $\mathbf{F}_c$  that obtain the same clique-homophily level  $h_c$ . We therefore choose the  $\mathbf{F}_c$  distribution that maximizes entropy for a given  $h_c$ . A maximum entropy distribution is the most unbiased distribution that satisfies the given constraints—in this case, the expected number of red nodes in a clique and the desired level of homophily. In networks with strong homophily, the distribution will favor cliques where nodes of the same color are grouped together, reflecting this tendency. In more heterogeneous networks, the distribution will allow for a

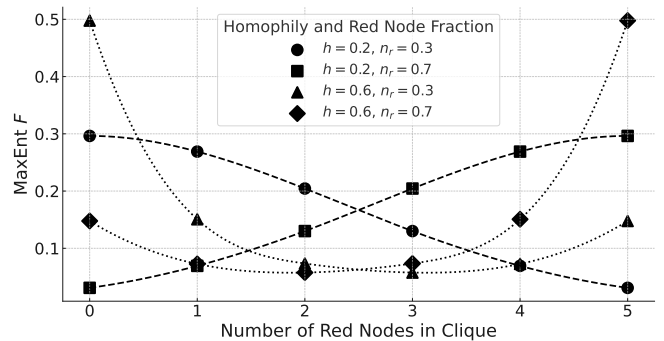


FIG. 2. The maximum entropy distribution  $\mathbf{F}_c$  for cliques of size  $c = 5$  presented for homophily values  $h = 0.2$  (solid lines) and  $h = 0.6$  (dashed lines) across two fractions of red nodes  $n_r = 0.3$  and  $n_r = 0.7$ .

broader mix of colors in the cliques, supporting diverse connections between red and blue nodes.

The maximum entropy distribution  $\mathbf{F}_c$ , in this setting, is given by

$$F_{c,i} = \frac{1}{Z} \exp(\theta_1 i + \theta_2 h_{c,i}). \quad (7)$$

The partition function  $Z$  normalizes the distribution  $\mathbf{F}_c$  after applying the other constraints.  $\theta_1$  and  $\theta_2$  are constants that are obtained by imposing that the average fraction of red nodes in the cliques balance with the total fraction of red nodes in the network,  $N_r$ , and that a desired homophily index,  $h_c$ , is achieved by the network.

In the large-network limit, Eq. (6) guarantees that after sampling the  $M_c$  cliques the proportion of red and blue nodes in the cliques coincides with the prescribed proportion of red and blue nodes in the network. In turn, average degrees for red and blue nodes coincide,

$$\langle k_r \rangle = \langle k_b \rangle = \langle k \rangle = M_c \frac{c(c-1)}{N}. \quad (8)$$

### B. Group Homophily

The final network  $G$  is constructed by combining various subgraphs  $G_c$ , represented as  $G = \bigcup_c G_c$ . Trivially,  $G_1$  is a graph composed of  $N$  isolated colored nodes and  $G_2$  is a stochastic block model (SBM) that accounts for the global homophily,  $h_g := h_2$ . For  $c > 2$ ,  $G_c$  includes homophilic groups, which exhibit local homophily,  $h_c$ . The total homophily of the network,  $h$ , is determined by both global and local homophilies:  $h = h(h_2, h_3, h_4, \dots)$ .

Each  $G_c$  contributes links to the final network  $G$ , with larger  $c$  values increasing the expected node degree significantly. We control the average degree of the combined network  $G$  by adjusting the number of samples  $M_c$  of different clique sizes. In the limit of large network size, for not very large  $c$ , if  $M_c$  does not grow faster than  $N$ ,

each network layer  $G_c$  contains  $M_c \frac{c(c-1)}{2}$  edges. Specifying the clique sizes, the total average degree for graph  $G$  is then given by

$$\langle k \rangle = \sum_c M_c \frac{c(c-1)}{N}. \quad (9)$$

Larger cliques influence the average degree more strongly. For this reason, in the large-network limit, the interesting case is when each clique size contributes to  $G$  with a similar amount of edges. This happens when we set the number of cliques  $M_c$  to scale inversely proportional to the number of edges in a single clique of size  $c$ . In particular, taking

$$M_c = \frac{N \langle k \rangle}{c(c-1)} \alpha_c, \quad (10)$$

where  $\sum_c \alpha_c = 1$ , we can tune the contribution to the average degree from cliques of any size  $c$  by tuning the parameter  $\alpha_c \in [0, 1]$ . The vector  $(\alpha_2, \alpha_3, \alpha_4, \dots)$  encodes the proportion of edges in the graphs coming from cliques of all different sizes, which makes it possible to compute the total homophily in the graph from the prescribed global and local homophily vector  $(h_2, h_3, h_4, \dots)$ :

$$h = \langle \alpha_c, h_c \rangle = \sum_{c \geq 2} \alpha_c h_c. \quad (11)$$

As an example, when  $G$  is obtained by combining only two clique networks  $G_c$  and  $G_{c'}$ , we weigh the contribution given by cliques of size  $c$  and  $c'$  by tuning the parameter  $\alpha_c$  and  $\alpha_{c'}$ . For instance, we can focus on the case  $G = G_2 \cup G_c$ , with  $c > 2$ , where given the desired average degree  $\langle k \rangle$  and the vector  $(\alpha_2, \alpha_c)$  we use Eq. 10 the number of 2-clique and  $c$ -cliques to sample. When  $\alpha_c < \alpha_2$ , global homophily is dominant and at  $\alpha_2 = \alpha_c = 0.5$ ,  $h$  represents the average of  $h_c$  and  $h_2$ . For  $\alpha_2 < \alpha_c$ , local homophily induced by  $c$ -cliques becomes dominant instead.

In the appendix, Fig. 12 showcases three network configurations: the first two with an equal number of cliques and the third with equal links from both clique types, demonstrating the impact of varying local and global homophily values on the overall network structure.

### C. Beyond two colors

So far, for the sake of simplicity, we have focused on networks where nodes possess binary attributes, such as male and female or red and blue. However, this framework can be extended to nodes with any discrete set of states or attributes, not just binary ones. Each clique network  $G_c$ , and consequently the mixed clique network  $G = \bigcup G_c$ , can be extended to a multi-color version. Assume that each node has one of the  $s \geq 1$  different colors, hence  $s(s+1)/2$  different edge types can be present. Different colors may represent different social groups, features, or functionalities within the network. The number

of vertices of each color is denoted by  $N_1, \dots, N_s$ , while their fraction over the total number of nodes  $N$  is denoted by  $n_1, \dots, n_s$ .

For fixed clique size  $c$ , each clique type can be uniquely specified by a vector  $\mathbf{i} = (i_1, \dots, i_s)$  encoding the number of vertices of each color in the clique. For example, if  $s = 3$  (red, blue, or green nodes) and  $c = 4$ , the vector  $(2, 1, 1)$  corresponds to the 4-clique with 2 red nodes, 1 blue node, and 1 green node. Similarly, as in the 2 color case, different cliques yield different homophily indices:

$$h_{\mathbf{i}} = \frac{\binom{i_1}{2} + \dots + \binom{i_s}{2}}{\binom{c}{2}} - \frac{(n_1^2 + \dots + n_s^2)}{1 - (n_1^2 + \dots + n_s^2)}.$$

$M_c$  cliques are sampled according to a given distribution vector  $\mathbf{F}_c$ , where  $F_{\mathbf{i}}$  specifies the probability of selecting a particular clique type. Constrained with achieving a desired network homophily value  $h$ , and assuming that all different color nodes have the same expected degree, we define the maximum entropy clique distribution

$$F_{\mathbf{i}} = \frac{1}{Z} \exp(\theta_1 i_1 + \dots + \theta_{s-1} i_{s-1} + \lambda h_{\mathbf{i}}).$$

The exponents  $\theta_1, \dots, \theta_{s-1}$  are conjugated to the constraints that ensure the average proportion of colored nodes in the cliques match the total proportion of colored cliques. Instead,  $\lambda$  is specified after requiring the desired homophily network value  $h$ . The constraints read explicitly as

$$N_j = \frac{1}{c} \sum_{\mathbf{i}} i_j F_{\mathbf{i}}, \quad j = 1, \dots, s-1 \quad (12)$$

$$h = \sum_{\mathbf{i}} h_{\mathbf{i}} F_{\mathbf{i}} \quad (13)$$

Similarly as in the 2-colored version, a multi-layer structured network can be obtained when mixing cliques of different sizes.

## III. EMPIRICAL NETWORKS

To evaluate how effectively our model captures real-world social network structures, we focus on datasets with gender attributes, analyzing how homophily varies across cliques of different sizes. We show two examples from the real world examples in the next section and leave more examples in the appendix. For each dataset, we identified all maximal cliques, grouped them by size  $c$ , and derived an empirical distribution representing the proportion of cliques containing varying numbers of red nodes. Our analysis assumes a maximum entropy distribution for clique configurations, constrained by the observed data, including the expected number of red nodes per clique and the overall homophily index. The inferred parameters  $\theta_1$  and  $\theta_2$ , define the shape of the maximum entropy distribution given by Eq. 7 that best fits the

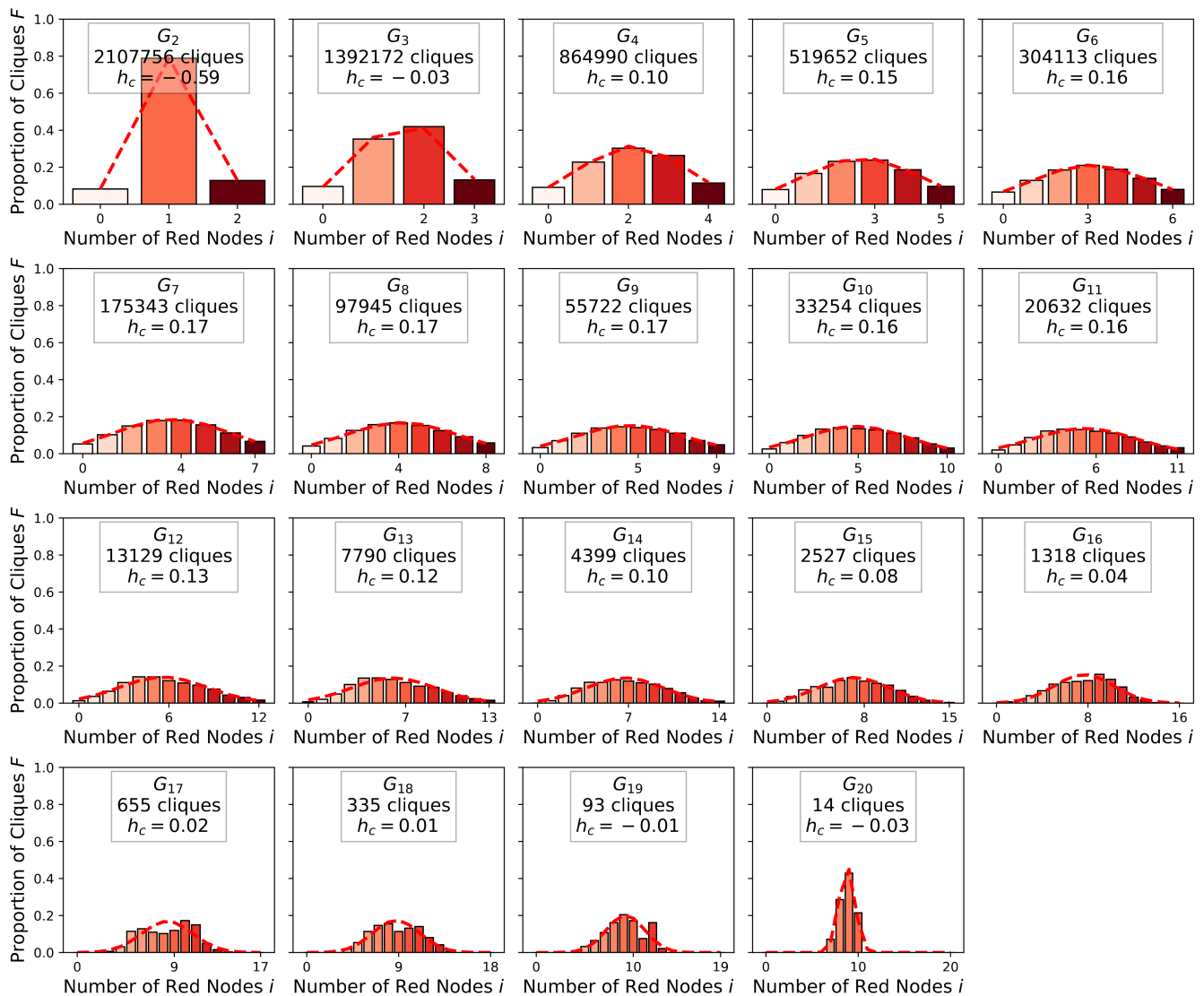


FIG. 3. Empirical and inferred distributions of  $\mathbf{F}_c$  for the local homophily for Pokec network with 53.42% red and 46.58% blue nodes (gender attributes) and Coleman homophily index  $h = -0.2$  given by Eq. 1. Each subpanel shows the empirical distribution of clique compositions by the number of red nodes, with the inferred maximum entropy distribution overlaid as a dotted line. Pokec remains Slovakia’s top online social network, thriving for over a decade despite competition from platforms like Facebook.

empirical data. By maximizing the likelihood of the observed distributions, we gain insight into local and global homophily values. The simplicity of exponential models makes this approach particularly effective for analyzing configurations with small numbers of states, as reflected in the remarkably close alignment between the observed data and the estimated distributions (dashed curves in Fig. 3).

To ensure the robustness of our estimates, we applied a bootstrap resampling procedure. For each clique size  $c$ , we resampled  $n_c$  cliques (equal to the observed count for that size) 1,000 times, generating a distribution of homophily values. This allowed us to compute mean homophily and construct 95% confidence intervals. These

results were visualized by plotting  $h_c$  against clique size, with error bars representing the confidence intervals, providing a clear view of how homophily evolve with clique size (see, for example, Fig. 4).

### A. Pokec Social Network

Pokec is a popular Slovak social networking platform that is widely used for social interactions and dating. The Pokec social network dataset, collected in 2012 from the Stanford Network Analysis Project (SNAP), contains 383,943 nodes representing users [29]. Of these users, 53.42% are labeled as red (female) and 46.58% are la-

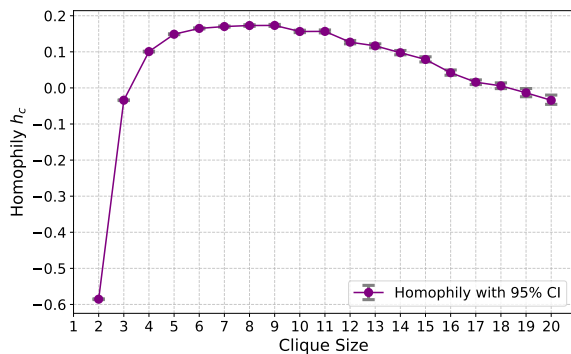


FIG. 4. The changes in  $h_c$  for the Pokec dating social media highlights the initial heterophily, preference for dating the opposite genders (colors), and the shift toward a more mixed structure in larger cliques as interactions become less gender-specific. Error bars represent 95% confidence intervals calculated using bootstrap resampling of cliques for each clique size.

beled as blue (male). The links between nodes represent friendship relationships. Fig. 3 displays the actual and estimated distribution of  $\mathbf{F}_c$  in each clique layer  $G_c$ . This network starts with a case of heterophily ( $G_2$ ), indicating that people on the Pokec platform tend to date others who are different from themselves. As the clique size increases, the network ends up having a very mixed structure for non-dyadic relationships. Fig. 4 illustrates how the tendency for heterophily decreases as people interact less dominantly with the opposite gender as the clique size grows.

## B. 100 Facebook Friendship Networks

In September 2005, a dataset on Facebook friendship networks from 100 universities in the US was collected as part of a study on homophily [30]. Fig. 5 shows the mean homophily versus clique size for these networks. It shows that larger cliques have higher homophily on average. In the appendix, Fig. 20 breaks down the analysis by the six most common available cliques. Each panel focuses on a specific maximal clique size, displaying an almost increasing scheme. In Appendix. B, we show similar distributions as for the Last.fm networks for US universities. For example, Fig.21 illustrates the situation for the Oberlin College network.

## IV. COLORED PERCOLATION

Group structures and homophily—where individuals preferentially connect with similar others—significantly constrain spreading phenomena and the diffusion of innovations and behaviors within social networks [2, 31–33]. For example, people get together in households, schools, and tight-knit communities, and this can push

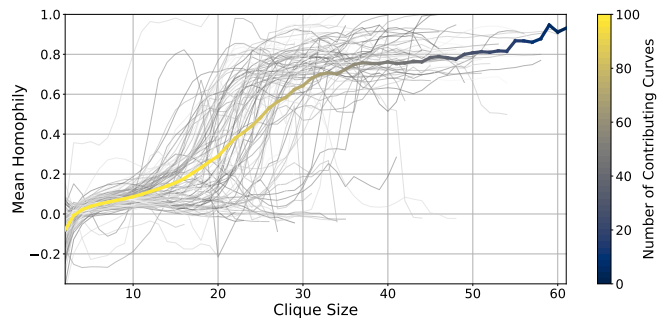


FIG. 5. Homophily VS clique size for Facebook friendship networks from 100 US universities. The larger the cliques, the larger the averaged homophily. This graph is divided into segments based on the number of available clique sizes for each network. The color shifts indicate the number of networks contributing to each segment, with lighter colors representing more networks. The background curves, shown in shades of gray, represent individual university networks. The color bar shows the number of contributing cases per segment.

the epidemic threshold, by acting as localized barriers to the spread of diseases, thereby reducing the risk of widespread outbreaks [34–37].

Understanding percolation processes, where nodes or links can be removed through various mechanisms, provides valuable insights into how network structures and connectivity change under different conditions [38, 39]. This understanding is crucial to predict epidemic thresholds and the likelihood of contagion spread. Moreover, it is instrumental in evaluating the effectiveness of different public health strategies and designing efficient immunization strategies [22, 23, 35, 37, 40–44].

Deriving analytical criteria for the connectivity of our network model is challenging. However, it is intuitive that the emergence of a giant connected component, which scales with the network size, requires a higher density of edges as clique size increases. Larger cliques inherently promote localized connections, which, while strengthening cohesion within groups, increase the risk of network fragmentation by limiting inter-group links. This trade-off highlights the delicate balance between clustering and global connectivity in such network structures.

Consider a scenario where red-red links remain active with probability  $\pi_{rr}$ , blue-blue links with probability  $\pi_{bb}$ , and red-blue links with probability  $\pi_{br}$ . In this case, assuming  $\pi_{br} = \pi_{bb} = 0$  and  $\pi_{rr} = p \leq 1$ , the colored percolation process is governed only by the spreading among red individuals. Under these conditions, the size of each group, along with local and global homophily, becomes significant. Fig. 6 demonstrates that higher homophily values—especially local homophily—lower the critical probability in the transmission network. Consequently, increased homophily reduces the epidemic threshold, making herd immunity more challenging to achieve, as expected [23]. All simulations and numerical

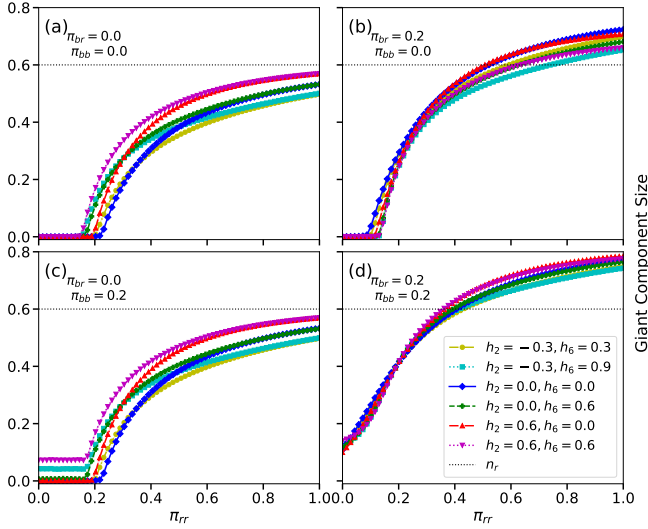


FIG. 6. Phase transition in the giant component of transmission networks with average degree six where red-red links are active with probability  $\pi_{rr}$ , and (a) all blue-blue and blue-red links removed,  $\pi_{rb} = 0.0$ ,  $\pi_{bb} = 0$ , (b)  $\pi_{rb} = 0.2$ ,  $\pi_{bb} = 0$ , (c)  $\pi_{rb} = 0.0$ ,  $\pi_{bb} = 0.2$ , (d)  $\pi_{rb} = \pi_{bb} = 0.2$ . The higher the homophily values, especially strong (local) homophily, the lower the critical probability. In (a) and (c), when  $\pi_{rr} = 1$ , the transmission network only includes the red-red links, and these links contain a portion of the red nodes such that the larger the homophily, the larger this portion. In the extreme case of  $h = 1$ , where the network is segregated, the red-red links contain  $N_r$  red nodes. Note that at this extreme, the larger the weak (global) homophily, the larger the giant component. For smaller  $n_r$  values, the separations between the curves become more pronounced.

computations are publicly available at [45].

### A. Critical percolation value

To analyze the critical percolation value numerically, we map the percolation process on the clique network to a percolation process on a tree-like network, by analyzing the spreading within the clique separately from the behavior between cliques. We therefore compute the average number of infected  $I'$ -cliques that are caused by a percolated vertex in an  $I$ -clique.

The average number of type  $I$ -cliques that are adjacent to a randomly chosen red or blue vertex equals

$$F_{r,I}^* := M_{c(I)} \frac{n_{r,I} F_I}{N_r}, \quad F_{b,I}^* := M_{c(I)} \frac{n_{b,I} F_I}{N_b}, \quad (14)$$

where  $n_{r,I}, n_{b,I}$  denote the number of red, blue nodes in a type  $I$  clique, and  $M_{c(I)}$  the total number of cliques of the same size as  $I$ . Furthermore, let  $\boldsymbol{\pi} = [\pi_{rr}, \pi_{rb}, \pi_{bb}]$  be the values quantifying the probabilities that red-red, red-blue, and blue-blue links are kept active after percolation. Finally, let  $g_r(I, \boldsymbol{\pi}, n_r, n_b)$  denote the probability that, after percolation, a randomly chosen red node is

still connected to  $n_r$  red and  $n_b$  blue nodes within the same clique of type  $I$ ; similarly,  $g_b(I, \boldsymbol{\pi}, n_r, n_b)$  denotes the probability for a randomly chosen blue node to remain connected to  $n_r$  and  $n_b$  nodes within  $I$ .

Then, the average number of type  $I'$  cliques that are reached after percolation from a node of color  $(*) \in \{r, b\}$  from a red node in a clique of type  $I$  equals

$$B_{I_r, I'_{(*)}} = F_{I', I'}^* \sum_{n_b=0}^{n_{b,I}} \sum_{n_r=1}^{n_{r,I}} (n_{(*)} - \delta_{r, (*)}) g_r(I, \boldsymbol{\pi}, n_r, n_b). \quad (15)$$

The term inside the inner summation is the average number of nodes of color  $(*)$  in the  $I$ -clique that are still connected to the red node after percolation. The term in front is the average number of type  $I'$  cliques adjacent to  $(*)$  colored nodes. The average number of  $I'$  cliques reached at a node of color  $(*)$  from a blue node in  $I$  is denoted by  $B_{I_b, I'_{(*)}}$ , and it is similarly computed.

Therefore, the matrix  $\mathbf{B} = \mathbf{B}(\boldsymbol{\pi})$  encodes the average number of vertices of specific clique types that are reached through percolation starting within another specific clique type. Then a percolation vector  $\boldsymbol{\pi}$  is critical when there is a vector  $\mathbf{v}$ , for which

$$\mathbf{v} \in \ker[\mathbf{B}(\boldsymbol{\pi}) - \mathbf{I}], \quad \mathbf{v}/|\mathbf{v}| \geq 0, \quad (16)$$

where  $\mathbf{I}$  denotes the identity matrix. Note that  $\det(\mathbf{B}(\boldsymbol{\pi}) - \mathbf{I}) = 0$  is a necessary condition for this to hold.

The elements of the matrix  $\mathbf{B}$  require the probabilities  $g_b(I, \boldsymbol{\pi}, n_r, n_b)$  and  $g_r(I, \boldsymbol{\pi}, n_r, n_b)$ . For any clique of type  $I$  with  $n_{r,I}$  red nodes and  $n_{b,I}$  blue nodes, the probability that the clique remains connected after percolation is  $g_b(I, \boldsymbol{\pi}, n_{r,I}, n_{b,I}) = g_r(I, \boldsymbol{\pi}, n_{r,I}, n_{b,I})$ . This probability equals to one minus the probability that there exists a cut in the clique, and can be written recursively as

$$\begin{aligned} g_b(I, \boldsymbol{\pi}, n_{r,I}, n_{b,I}) &= 1 - \sum_{j=1}^{n_{b,I}} \sum_{i=0}^{n_{r,I}} \binom{n_{b,I}-1}{j-1} \binom{n_{r,I}}{i} \\ &\times g_b(I_{i,j}, \boldsymbol{\pi}, i, j) (1 - \pi_{rr})^{i(d_r-i)} \\ &\times (1 - \pi_{bb})^{j(d_b-j)} (1 - \pi_{br})^{i(d_b-j)+j(d_r-i)}, \end{aligned} \quad (17)$$

$$\begin{aligned} g_r(I, \boldsymbol{\pi}, n_{r,I}, n_{b,I}) &= 1 - \sum_{j=0}^{n_{b,I}} \sum_{i=1}^{n_{r,I}} \binom{n_{b,I}}{j} \binom{n_{r,I}-1}{i-1} \\ &\times g_b(I_{i,j}, \boldsymbol{\pi}, i, j) (1 - \pi_{rr})^{i(d_r-i)} \\ &\times (1 - \pi_{bb})^{j(d_b-j)} (1 - \pi_{br})^{i(d_b-j)+j(d_r-i)}. \end{aligned} \quad (18)$$

From these equations, we can compute  $g_b(I, \boldsymbol{\pi}, n_r, n_b)$  when  $n_r \leq n_{r,I}$  or  $n_b \leq n_{b,I}$ , as

$$\begin{aligned} g_b(I, \boldsymbol{\pi}, n_r, n_b) &= \binom{n_{b,I}-1}{n_b-1} \binom{n_{r,I}}{n_r} g_b(I_{n_r, n_b}, \boldsymbol{\pi}, n_r, n_b) \\ &\times (1 - \pi_{rr})^{n_r(n_{r,I}-n_r)} (1 - \pi_{bb})^{n_b(n_{b,I}-n_b)} \\ &\times (1 - \pi_{br})^{n_r(n_{b,I}-n_b)+n_b(n_{r,I}-n_r)}, \end{aligned} \quad (19)$$

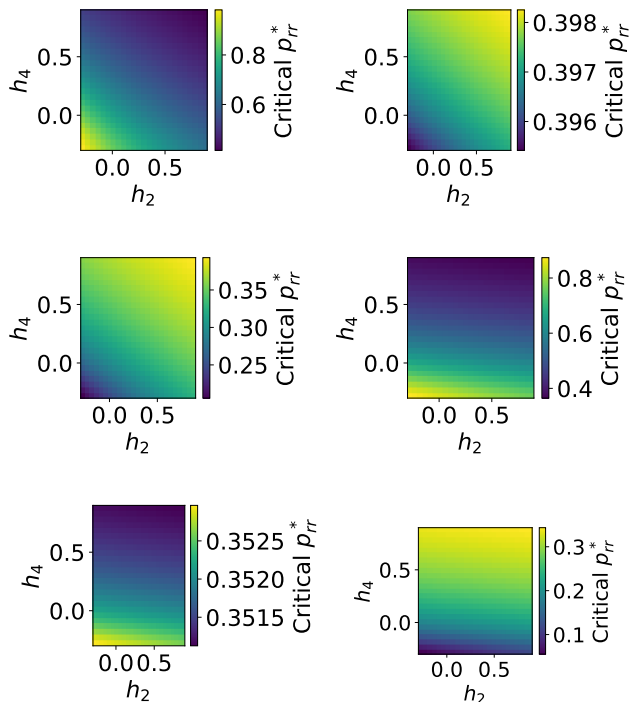


FIG. 7. Transition in the effect of local homophily on the critical percolation value. Critical value for  $\pi_{bb} = \pi_{rr}$   $c = 4$ ,  $N_r/N = 0.5$ ,  $\alpha = \alpha^*$  (in a), b), c)), average degree 2. a)  $\pi_{rb} = 0.1$  b)  $\pi_{rb} = 0.4$ , c)  $\pi_{rb} = 0.5$ . In d), e), f)  $\alpha = 0.5$  d)  $\pi_{rb} = 0.1$  e)  $\pi_{rb} = 0.35$ , f)  $\pi_{rb} = 0.5$ ,

$$\begin{aligned}
 g_r(I, \boldsymbol{\pi}, n_r, n_b) &= \binom{n_{b,I}}{n_b} \binom{n_{r,I} - 1}{n_r - 1} g_r(I_{n_r, n_b}, \boldsymbol{\pi}, n_r, n_b) \\
 &\times (1 - \pi_{rr})^{n_r(n_r, I - n_r)} (1 - \pi_{bb})^{n_b(n_b, I - n_b)} \\
 &\times (1 - \pi_{br})^{n_r(n_b, I - n_b) + n_b(n_r, I - n_r)}. \quad (20)
 \end{aligned}$$

These equations takes the probability that a clique with  $n_r$  and  $n_b$  red and blue vertices remains connected from Eq. (17) and (18), and multiplies it with the probability that these vertices are not connected to any remaining vertices of the clique.

Fig. 7 shows a heatmap of the critical percolation value with respect to the two homophily parameters. We see that the choice of  $\alpha$  is crucial in determining the effect that the two homophilies have on the critical value. Indeed, when  $\alpha$  is larger (Figures d, e, f), there are more edges within 4-cliques than in 2-cliques, and the effect of the 4-cliques dominates the critical percolation value. When there are as many edges in 4-cliques as in 2-cliques (Figures a, b, c), both homophilies equally affect the critical value. The effect of the interplay between the different percolation probabilities between and within colors is more interesting. When  $\pi_{rb}$  is low, increasing homophily decreases the critical percolation value. On the other hand, when  $\pi_{rb}$  is large, it increases the critical percolation value.

We now compare the critical percolation values and

the impact of the different types of homophily. By introducing the two levels of homophily, there are multiple ways to achieve the same total homophily value  $h$  given by Eq. (11). We now investigate the impact of choosing different local homophily levels that lead to the same total homophily on the critical percolation value. In particular, we fix  $h^*$ . Then, two possible ways to achieve a particular homophily value  $h$  are setting  $h_4 = h^*$  and fix  $h_2$  to match the total homophily  $h$  using Eq. (11). A second way is to fix  $h_2 = h^*$  and match  $h_4$  to obtain total homophily  $h$ . We then compute the critical percolation value  $\pi_{rr}^*(h_4 = h^*)$ , for given  $\pi_{rb}$  and setting  $\pi_{bb} = \pi_{rr}$ . We compare this critical percolation value to the critical  $\pi_{rr}(h_2 = h^*)$  at the same total homophily  $h$ . The difference between these two values indicates the impact that the layers of homophily may have on the critical percolation value. Fig. 8 shows that the different layers of homophily may have a large impact on the percolation value. Interestingly, this effect has non-trivial behavior in the parameter space. When  $\pi_{rb}$  is small, a higher value of clique homophily may lead to lower percolation values, but for larger  $\pi_{rb}$  this effect reverses.

Fig. 7 shows that the value of  $\pi_{rb}$  at which the effect of local homophily reverses in Fig. 8 is exactly where the effect of changing the different homophily is almost zero. Indeed, for example, Fig. 8a changes effect in the parameter  $\pi_{rb}$  from negative to positive approximately at  $\pi_{rb} = 0.4$ . Fig. 7b shows that indeed at that value, the effect of changing either of the two homophilies is close to zero. Similarly, in Fig. 8, the transition is around  $\pi_{rb} = 0.35$ , and Fig. 7e shows that the effect of changing homophily is indeed close to zero.

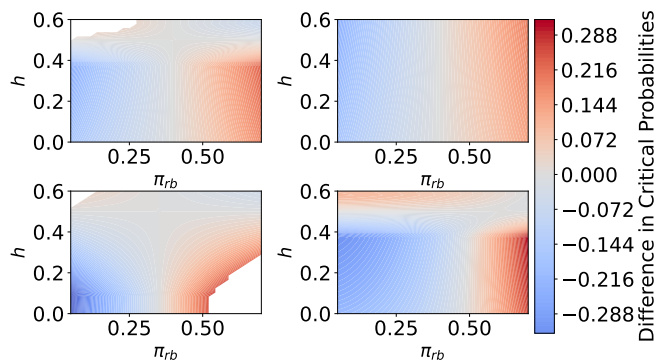


FIG. 8. The effect of local homophily levels on percolation. Area plot of  $\pi_{rb}$  against total homophily  $h$ . The color value indicates the value of  $\pi_{rr}^*(h_4 = h^*) - \pi_{rr}^*(h_2 = h^*)$  value, when  $\pi_{bb} = \pi_{rr}$ ,  $c = 4$ , average degree is 2,  $N_r/N = 0.5$ . Red indicates that setting  $h_4 = h^*$  and  $h_2$  so that the total homophily is  $h$  has a higher percolation value than setting  $h_2 = h^*$  and  $h_4$  to make the total homophily equal to  $h$ . a)  $h^* = 0.5$ ,  $\alpha = \alpha^*$  b)  $h^* = 1$ ,  $\alpha = \alpha^*$ , c)  $h^* = 0.5$ ,  $\alpha = 0.5$ . d)  $\pi_{bb} = 0.1\pi_{rr}$ . White area is where there is no critical percolation value, due to (1) no giant component in graph without percolation, (2) already a giant component when  $\pi_{rr} = 0$ .

We then investigate the effect of the different possible combinations of the inter and intra-color percolation parameters. Fig. 9 shows how different local homophily settings that give rise to the same total homophily may have different critical  $\pi_{rr}$  values for a specific  $\pi_{bb}$  and  $\pi_{rb}$ . In particular, the plot fixes the global homophily at  $h = 0$ . Then, it calculates the critical  $\pi_{rr}$  value for  $h_2 = h^*$ , and  $h_4$  such that the total homophily equals  $h$ ,  $\pi_{rr}^*(h_2 = h^*)$ , as well as the critical  $\pi_{rr}$  value for  $h_4 = h^*$ , and  $h_2$  such that the total homophily equals  $h$ ,  $\pi_{rr}^*(h_4 = h^*)$ . The figure plots  $\pi_{rr}^*(h_4 = h^*) - \pi_{rr}^*(h_2 = h^*)$ . The figure again shows a difference in effect for different inter and intra-color percolation parameters: for larger  $\pi_{rb}$  the effect of homophily is the reverse from the effect at lower  $\pi_{rb}$ . Furthermore, the interaction between the parameters  $\pi_{rb}$  and  $\pi_{bb}$  also plays a non-trivial role.

### B. Vaccination as an Example

We now consider a situation in which the red nodes correspond to vaccinated nodes, and the blue nodes to unvaccinated nodes, under an imperfect vaccine.

Let the inter-group efficacy of the vaccine be  $f_I$ . That is, when the spreading probability between two unvaccinated nodes equals  $\pi$ , then the spreading probability between a vaccinated and an unvaccinated node equals  $\pi_{rb} = f_I\pi$ . The spreading probability between two vaccinated nodes equals  $\pi_{bb} = \pi f_I f_v$ . Fig. 10 shows the results for several values for  $f_I$  and  $f_v$ .

As in Fig. 7, we see that the effect of homophily on the critical percolation value can flip. For example, in Fig. 10b, where  $f_I = 0.1, f_v = 0.5$ , increasing any of the two local homophilies leads to a higher critical percolation value. In Fig. 10d on the other hand, where  $f_I = 1, f_v = 0.1$ , increasing homophily leads to a lower percolation value. This effect is consistent with the results in Fig. 7, where we saw that for low  $\pi_{rb}$ , increasing homophily leads to a lower critical probability, as in this case,  $\pi_{rb} = f_I\pi$ . In Fig. 10d, the red-blue percolation probability is  $\pi$ , while it is  $0.5\pi$  in Fig. 10b. Furthermore, Fig. 10a shows that again, there is some combination of  $f_I$  and  $f_v$  that makes the critical percolation probability almost independent of any local homophily.

In a tree-like network with homophily  $h$ , the required vaccine coverage (fraction of red nodes) for herd immunity is known to increase in  $h$ , with strong homophily potentially making the threshold unattainable [23]. Moreover, the size of the epidemic increases consistently with the strength of homophily for a perfect vaccine, whereas for a vaccine with limited efficacy, it peaks at a specific homophily level [23]. In contrast, our results show that the setting with multiple layers of homophily make the results much more intricate. This underscores the importance of accounting for vaccination homophily in epidemic modeling.

These insights show that in the case of vaccination, which creates unequal spreading probabilities between

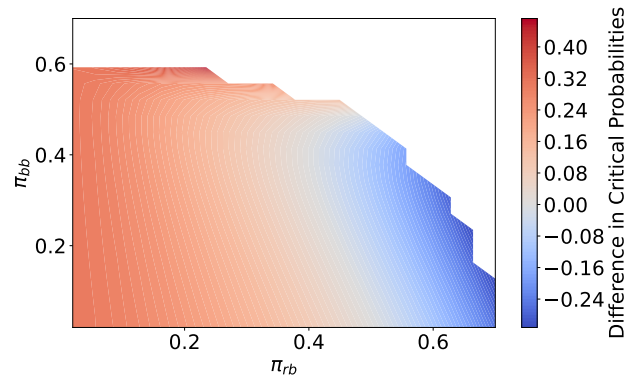


FIG. 9. Area plot of  $\pi_{rb}$  against  $\pi_{bb}$ . Red indicates that setting  $h_4 = h^*$  and  $h_2$  so that the total homophily is  $h$  has a higher percolation value than setting  $h_2 = h^*$  and  $h_4$  to make the total homophily equal to  $h$ . In this plot,  $\alpha = 0.5, h = 0, h^* = 0.1$ . In the white area, no critical value of  $\pi_{rr}$  exists for the given combination of  $\pi_{bb}$  and  $\pi_{rb}$ .

different groups, the critical value may be severely impacted by varying levels of different layered homophily. For example, in Fig. 10b, the critical percolation value ranges from 0.45 to 0.89, which is almost a factor two difference.

## V. CONCLUSION & DISCUSSION

The spread of information, behaviors, and contagions shapes public discourse, innovation, and health outcomes. Understanding these dynamics is crucial for effective interventions, whether for misinformation, technology diffusion, or disease transmission. Here we provided a nuanced understanding of how assortative mixing influences spreading phenomena, including information dissemination, fake news, innovation diffusion, and epidemics. The effectiveness of containment measures and epidemic interventions, particularly those with limited efficacy, depends heavily on homophilic structures.

Our research introduces a framework that considers different levels of homophily: between and within groups. This expands upon traditional social network models that mainly focus on pairwise interactions. We have shown that a maximum entropy approach is able to capture the homophily patterns in real-world data accurately. These findings have significant implications for improving public health strategies, managing misinformation on social media, and designing targeted interventions for both information control and epidemic containment.

We show that the effect of these levels of homophily on the percolation threshold is non-trivial: depending on the precise inter- and intra-group network parameters, inter or intra-group percolation may either increase or decrease the critical percolation value. Therefore, our model improves the accuracy of predicting epidemic spread and

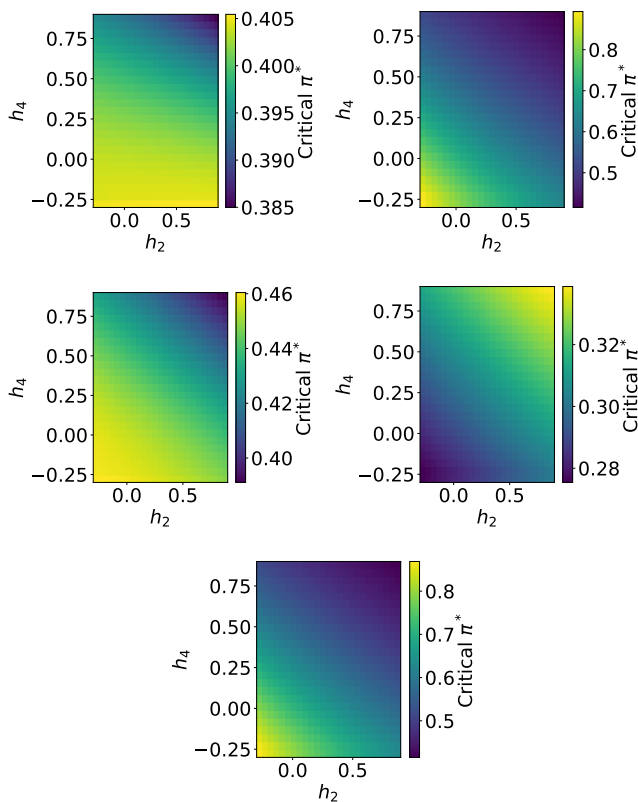


FIG. 10. Critical value  $\pi$  under vaccination with  $N_r/N = 0.6$ , average degree 2,  $\alpha = \alpha_c$ ,  $c_1 = 4$ ,  $c_2 = 2$ . The plots show the critical probability  $\pi$  for varying homophily levels. a)  $f_I = f_v = 0.5$ , b)  $f_I = 0.1$ ,  $f_v = 0.5$ , c)  $f_I = 0.5$ ,  $f_v = 0.1$  d)  $f_I = 1$ ,  $f_v = 0.1$ , e)  $f_I = 0.1$ ,  $f_v = 1$

underscores the crucial role of group interactions in refining intervention strategies such as targeted vaccinations and social distancing policies.

## ACKNOWLEDGMENT

The simulations presented above were performed using computer resources within the Aalto University School of Science “Science-IT” project. All simulations and numerical computations are publicly available at [45].

- 
- [1] M. E. Newman, Assortative mixing in networks, *Physical review letters* **89**, 208701 (2002).
  - [2] M. McPherson, L. Smith-Lovin, and J. M. Cook, Birds of a feather: Homophily in social networks, *Annual review of sociology* **27**, 415 (2001).
  - [3] M. Kalmijn, Intermarriage and homogamy: Causes, patterns, trends, *Annual review of sociology* **24**, 395 (1998).
  - [4] V. A. Lewis, Social energy and racial segregation in the university context, *Social Science Quarterly* **93**, 270 (2012).
  - [5] E. Bakshy, S. Messing, and L. A. Adamic, Exposure to ideologically diverse news and opinion on facebook, *Science* **348**, 1130 (2015).
  - [6] V. Oldemburgo de Mello, F. Cheung, and M. Inzlicht, Twitter (x) use predicts substantial changes in well-being, polarization, sense of belonging, and outrage, *Communications Psychology* **2**, 15 (2024).
  - [7] J. Tacchi, C. Boldrini, A. Passarella, and M. Conti, Keep your friends close, and your enemies closer: Structural properties of negative relationships on twitter, *arXiv:2401.16562* (2024).
  - [8] A. Porter and I. Rafols, Is science becoming more interdisciplinary? measuring and mapping six research fields over time, *Scientometrics* **81**, 719 (2009).
  - [9] M. Á. Serrano, M. Boguñá, and A. Vespignani, Patterns of dominant flows in the world trade web, *Journal of Economic Interaction and Coordination* **2**, 111 (2007).
  - [10] M. S. Granovetter, The strength of weak ties, *American journal of sociology* **78**, 1360 (1973).
  - [11] M. Granovetter, The strength of weak ties: A network theory revisited, *Sociological theory* , 201 (1983).
  - [12] H. Louch, Personal network integration: transitivity and homophily in strong-tie relations, *Social networks* **22**, 45 (2000).
  - [13] P. Preciado, T. A. Snijders, W. J. Burk, H. Stattin, and M. Kerr, Does proximity matter? distance dependence of adolescent friendships, *Social networks* **34**, 18 (2012).
  - [14] C. McMillan, Strong and weak tie homophily in adolescent friendship networks: An analysis of same-race and same-gender ties, *Network Science* **10**, 283 (2022).
  - [15] J. A. Yorke, H. W. Hethcote, and A. Nold, Dynamics and control of the transmission of gonorrhoea, *Sexually transmitted diseases* , 51 (1978).
  - [16] C. Buckee, A. Noor, and L. Sattenspiel, Thinking clearly about social aspects of infectious disease transmission, *Nature* **595**, 205 (2021).
  - [17] S. Patwardhan, V. K. Rao, S. Fortunato, and F. Radicchi, Epidemic spreading in group-structured populations,

- Physical Review X **13**, 041054 (2023).
- [18] C. McMillan, Worth the weight: Conceptualizing and measuring strong versus weak tie homophily, *Social networks* **68**, 139 (2022).
- [19] J. Moody, Race, school integration, and friendship segregation in america, *American journal of Sociology* **107**, 679 (2001).
- [20] S. M. Goodreau, J. A. Kitts, and M. Morris, Birds of a feather, or friend of a friend? using exponential random graph models to investigate adolescent social networks, *Demography* **46**, 103 (2009).
- [21] R. S. Burt, Structural holes, in *Social stratification* (Routledge, 2018) pp. 659–663.
- [22] A. K. Rizzi, A. Faqeeh, A. Badie-Modiri, and M. Kivelä, Epidemic spreading and digital contact tracing: Effects of heterogeneous mixing and quarantine failures, *Physical Review E* **105**, 044313 (2022).
- [23] T. Hiraoka, A. K. Rizzi, M. Kivelä, and J. Saramäki, Herd immunity and epidemic size in networks with vaccination homophily, *Physical Review E* **105**, L052301 (2022).
- [24] F. Battiston, E. Amico, A. Barrat, G. Bianconi, G. Ferraz de Arruda, B. Franceschiello, I. Iacopini, S. Kéfi, V. Latora, Y. Moreno, *et al.*, The physics of higher-order interactions in complex systems, *Nature Physics* **17**, 1093 (2021).
- [25] N. Veldt, A. R. Benson, and J. Kleinberg, Combinatorial characterizations and impossibilities for higher-order homophily, *Science Advances* **9**, eabq3200 (2023).
- [26] A. Sarker, N. Northrup, and A. Jadbabaie, Higher-order homophily on simplicial complexes, *Proceedings of the National Academy of Sciences* **121**, e2315931121 (2024).
- [27] J. S. Coleman, Relational Analysis: The Study of Social Organizations with Survey Methods, *Human Organization* **17**, 28 (1958).
- [28] J. S. Coleman, *Introduction to Mathematical Sociology* (Free Press of Glencoe, New York, 1964) pp. xiv, 554.
- [29] L. Takac and M. Zabovsky, Data analysis in public social networks, in *International scientific conference and international workshop present day trends of innovations*, Vol. 1 (2012).
- [30] A. L. Traud, P. J. Mucha, and M. A. Porter, Social structure of facebook networks, *Physica A: Statistical Mechanics and its Applications* **391**, 4165 (2012).
- [31] K. Z. Khanam, G. Srivastava, and V. Mago, The homophily principle in social network analysis: A survey, *Multimedia Tools and Applications* **82**, 8811 (2023).
- [32] D. Guilbeault, J. Becker, and D. Centola, Complex contagions: A decade in review, *Complex spreading phenomena in social systems: Influence and contagion in real-world social networks*, 3 (2018).
- [33] D. Centola, The spread of behavior in an online social network experiment, *science* **329**, 1194 (2010).
- [34] A. K. Rizzi, L. A. Keating, J. P. Gleeson, D. J. O’Sullivan, and M. Kivelä, Effectiveness of contact tracing on networks with cliques, *Physical Review E* **109**, 024303 (2024).
- [35] T. Hiraoka, A. K. Rizzi, Z. Ghadiri, M. Kivelä, and J. Saramäki, The strength and weakness of disease-induced herd immunity, *arXiv:2307.04700* (2023).
- [36] T. W. Valente, Network interventions, *science* **337**, 49 (2012).
- [37] R. Pastor-Satorras and A. Vespignani, Epidemic spreading in scale-free networks, *Physical review letters* **86**, 3200 (2001).
- [38] M. Newman, *Networks* (Oxford university press, 2018).
- [39] A. K. Rizzi, *Spreading and Epidemic Interventions - Effects of Network Structure and Dynamics*, Ph.d. thesis, Aalto University (2024).
- [40] C. Moore and M. E. Newman, Epidemics and percolation in small-world networks, *Physical Review E* **61**, 5678 (2000).
- [41] M. E. Newman, Spread of epidemic disease on networks, *Physical review E* **66**, 016128 (2002).
- [42] R. Cohen, S. Havlin, and D. Ben-Avraham, Efficient immunization strategies for computer networks and populations, *Physical review letters* **91**, 247901 (2003).
- [43] I. Kryven, Bond percolation in coloured and multiplex networks, *Nature communications* **10**, 404 (2019).
- [44] M. D. Penney, Y. Yargic, L. Smolin, E. W. Thommes, M. Anand, and C. T. Bauch, “hot-spotting” to improve vaccine allocation by harnessing digital contact tracing technology: An application of percolation theory, *Plos one* **16**, e0256889 (2021).
- [45] Github repository, <https://github.com/k-rizzi/Homophily-Within-Across-Groups>.
- [46] P. Sapiezynski, A. Stopczynski, D. D. Lassen, and S. Lehmann, Interaction data from the copenhagen networks study, *Scientific Data* **6**, 315 (2019).
- [47] A. Asikainen, G. Iñiguez, J. Ureña-Carrión, K. Kaski, and M. Kivelä, Cumulative effects of triadic closure and homophily in social networks, *Science Advances* **6**, eaax7310 (2020).
- [48] J.-P. Onnela, J. Saramäki, J. Hyvönen, G. Szabó, D. Lazer, K. Kaski, J. Kertész, and A.-L. Barabási, Structure and tie strengths in mobile communication networks, *Proceedings of the National Academy of Sciences* **104**, 7332 (2007), <https://www.pnas.org/doi/pdf/10.1073/pnas.0610245104>.
- [49] A. Asikainen, G. Iñiguez, K. Kaski, and M. Kivelä, Cumulative effects of triadic closure and homophily in social networks, *arXiv:1809.06057* (2018).

## Appendix A: Network Statistics

The abundance of colored nodes and the shape of the distribution  $\mathbf{F}_c$  influence the degree of colored nodes. In the large-network limit, if the number of cliques scales linearly in the network size, the degree distributions of red and blue nodes can be approximated using Poisson distributions. The degree of a red nodes  $k_r$  follows a Poisson distribution with parameter  $\lambda_r$ .

$$\lambda_r = \frac{M}{N_r} \sum_{i=1}^c i F_{c,i}. \quad (\text{A1})$$

This results in the degree distribution

$$P(k_r = k) \approx \frac{\lambda_r^{k/(c-1)} e^{-\lambda_r}}{(k/(c-1))!}. \quad (\text{A2})$$

Similarly, for blue nodes, the degree  $k_b$  follows a similar Poisson distribution with parameter  $\lambda_b$

$$\lambda_b = \frac{M}{N_b} \sum_{i=0}^{c-1} (c-i) F_{c,i}. \quad (\text{A3})$$

The average degrees of red and blue nodes  $\langle k_r \rangle$  and  $\langle k_b \rangle$  depend on the choice of the clique distribution vector  $\mathbf{F}_c$ , and they can be different in principle. However, choosing the  $\mathbf{F}_c$  via the maximum entropy approach described earlier guarantees equal average degrees. This symmetric selection process ensures that both node types are equally likely to be included in cliques, thereby balancing their degree contributions.

Each clique of size  $c$  has  $\binom{c}{2}$  links. The number of red-red (rr), blue-blue (bb), and red-blue (rb) links depends on the number of red nodes  $i$  in the clique. The total number of rr, bb, and rb links before any link removal is given by  $l_{rr} = M \sum_{i=2}^c F_i^c \binom{i}{2}$ ,  $l_{bb} = M \sum_{i=0}^{c-2} F_i^c \binom{c-i}{2}$ , and  $l_{rb} = M \sum_{i=1}^{c-1} F_i^c (i(c-i))$ , respectively.

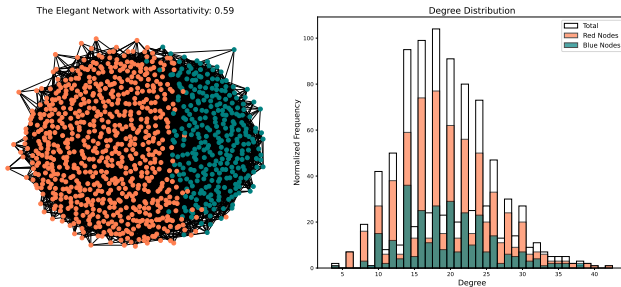


FIG. 11. Degree distribution of  $G_3$  (homophilic 3-clique networks) of size 1000 with 70% red nodes,  $h_3 = 0.6$  and average degree 20.

## Appendix B: Real Data

### 1. The Copenhagen Networks Study

The Copenhagen Networks Study dataset provides rich multi-layer network data collected from over 700 university students over a period of four weeks [46]. It contains data from several communication channels, including physical proximity (via Bluetooth where we set the signal strength threshold to -80 dBm), phone calls, SMS messages, and Facebook friendships. This gendered dataset captures highly interconnected groups, which naturally form cliques due to the frequent, repeated interactions between individuals in close proximity, such as students sharing dormitories or classrooms. We aggregated the data to gather all the four-week connectives into a static network. Fig. 23 shows the homophily situation in this network.

### 2. Last.fm Network

The dataset from the music-sharing platform Last.fm represents a snapshot of a self-reported friendship network, with 188,672 user connections and associated gender information. This friendship network has an average degree of 5.5 and is divided into two groups based on gender. Only users with available gender data detected from their names are included, where red represents gender one and blue represents gender two [47]. Fig. 14 illustrates the distribution  $\mathbf{F}_c$  across all subgraphs derived from this network.

### 3. Mobile Phone Data

Mobile phone network of a major European carrier is based on call detail records, where two individuals are connected if they have called each other at least once during a one-year observation period [48]. Ref.[49] shows that the network exhibits homophily, with the smaller female group displaying some homophily amplification.

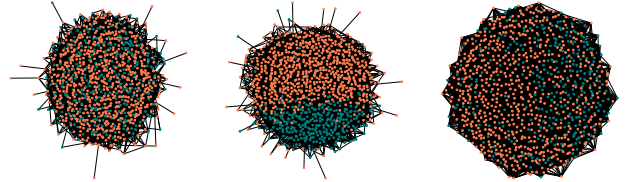


FIG. 12.  $G_{2,6}$ , a homophilic network of 2 and 6-cliques of size 1000 with 70% red nodes and an average degree of 20, where same number of samples have taken and (a)  $h_2 = -0.1$ ,  $h_6 = 0.6$ , and  $h = -0.06$ ; (b)  $h_2 = 0.6$ ,  $h_6 = -0.1$ , and  $h = 0.54$ ; and different number of samples have taken but (c)  $h_2 = 0.6$ ,  $h_6 = -0.1$ , and  $h = 0.25$ .

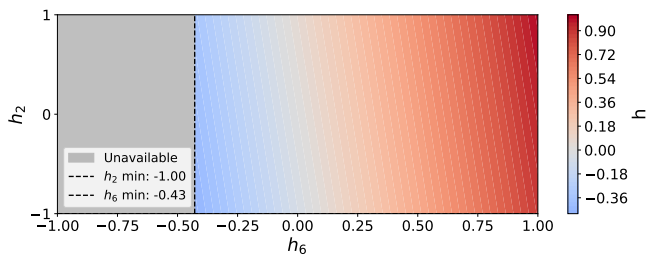


FIG. 13. Homophily values,  $h = \frac{1}{16}(h_2 + 15h_6)$ , for a network with 2 and 6-cliques and 70% red nodes. The gray area represents impossible heterophilic structures as bounded by Eq. 3.

However, for the larger male population, the observed homophily may be underestimated due to the triadic closure mechanism. This means that while women may form more connections within their own group, the connections among men may appear less homophilic because the mechanism of triadic closure plays a role in how connections are formed.

Fig.21 illustrates the situation for the Oberlin College network. Additionally, Fig.15 shows the Duke University network, Fig.16 represents the UCSD network, Fig.17 displays the Simmons University network, Fig.18 illustrates the Wellesley College network, and Fig.19 depicts the Wesleyan University network.

### Appendix C: Percolation

After link removal, where rr links are kept with probability  $\pi_{rr}$ , bb links with  $\pi_{bb}$ , and rb links with  $\pi_{rb}$ , the expected number of remaining rr, bb, and rb links becomes  $l_{rr}\pi_{rr}$ ,  $l_{bb}\pi_{bb}$ , and  $l_{rb}\pi_{rb}$ , respectively. The expected number of surviving cliques is

$$M \sum_{i=0}^c F_i^c \pi_{rr}^{\binom{i}{2}} \pi_{bb}^{\binom{c-i}{2}} \pi_{rb}^{i(c-i)}, \quad (C1)$$

where a clique with  $i$  red nodes has  $\binom{i}{2}$  rr links,  $\binom{c-i}{2}$  bb links, and  $i(c-i)$  rb links.

Percolation thresholds varies differently according to weak and strong homophily.

### 1. Percolation Process Implementation

According the network model, the probability of a red node being placed in a clique and forming connections with other red nodes is controlled by the Coleman homophily index, calculated for each clique. Similarly, blue nodes were clustered together with the same approach. To perform the percolation process, we sampled edges from the network according to the edge type: red-red ( $\pi_{rr}$ ), red-blue ( $\pi_{rb}$ ), and blue-blue ( $\pi_{bb}$ ). These edge types represent the probabilities of retaining each type of edge during the percolation process. Specifically, for a given edge type, a fraction  $\pi$  of the edges is retained, and the remaining edges are removed. This allows us to explore how the connectivity between different node types influences the overall network structure.

At each step in the percolation process, for a given probability  $\pi_{rr}$  of retaining red-red edges, the largest connected component (i.e., the giant component) and susceptibility were measured. The giant component was calculated as the fraction of nodes in the largest connected component, while the susceptibility was computed as the average size of the remaining components excluding the giant component,  $\chi = \langle \sigma \rangle$ . This definition of susceptibility gives a smoother behavior for the simulated curves. Moreover, homophilic connections, particularly through  $\pi_{bb} > 0$ , caused an interesting behavior where the average size of small components grew after the percolation point, influencing the tail behavior of the susceptibility curves. To ensure robustness, we performed ensemble averaging over multiple network realizations and computed the mean size of the giant component and the susceptibility as a function of the percolation probability. This approach allows us to identify the critical percolation threshold  $\pi^*$ , where the giant component rapidly forms, as the first local maximum of the susceptibility curve. The heatmaps shows such values in different parameter settings.

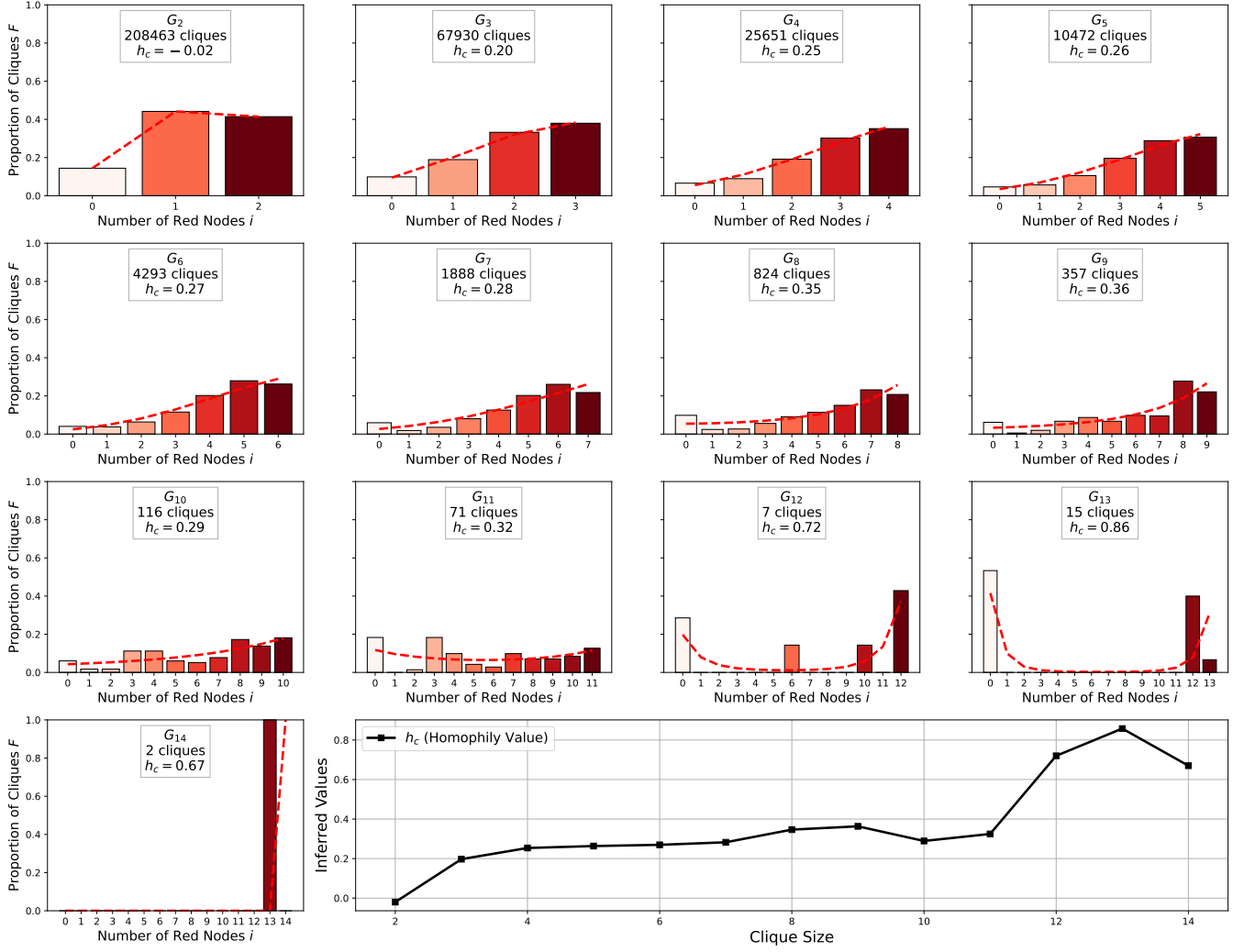


FIG. 14. Local homophily distributions for Last.fm network with 32% red nodes, constructed from subnetworks  $G_2, G_3, \dots, G_{14}$ . Each subpanel shows the empirical distribution of clique compositions by the number of red nodes, with the inferred maximum entropy distribution overlaid as a dotted line. The last panel (bottom-right) displays the inferred homophily values  $h_c$  based on Eq. 5 and parameters  $\theta_1, \theta_2$  as a function of clique size.

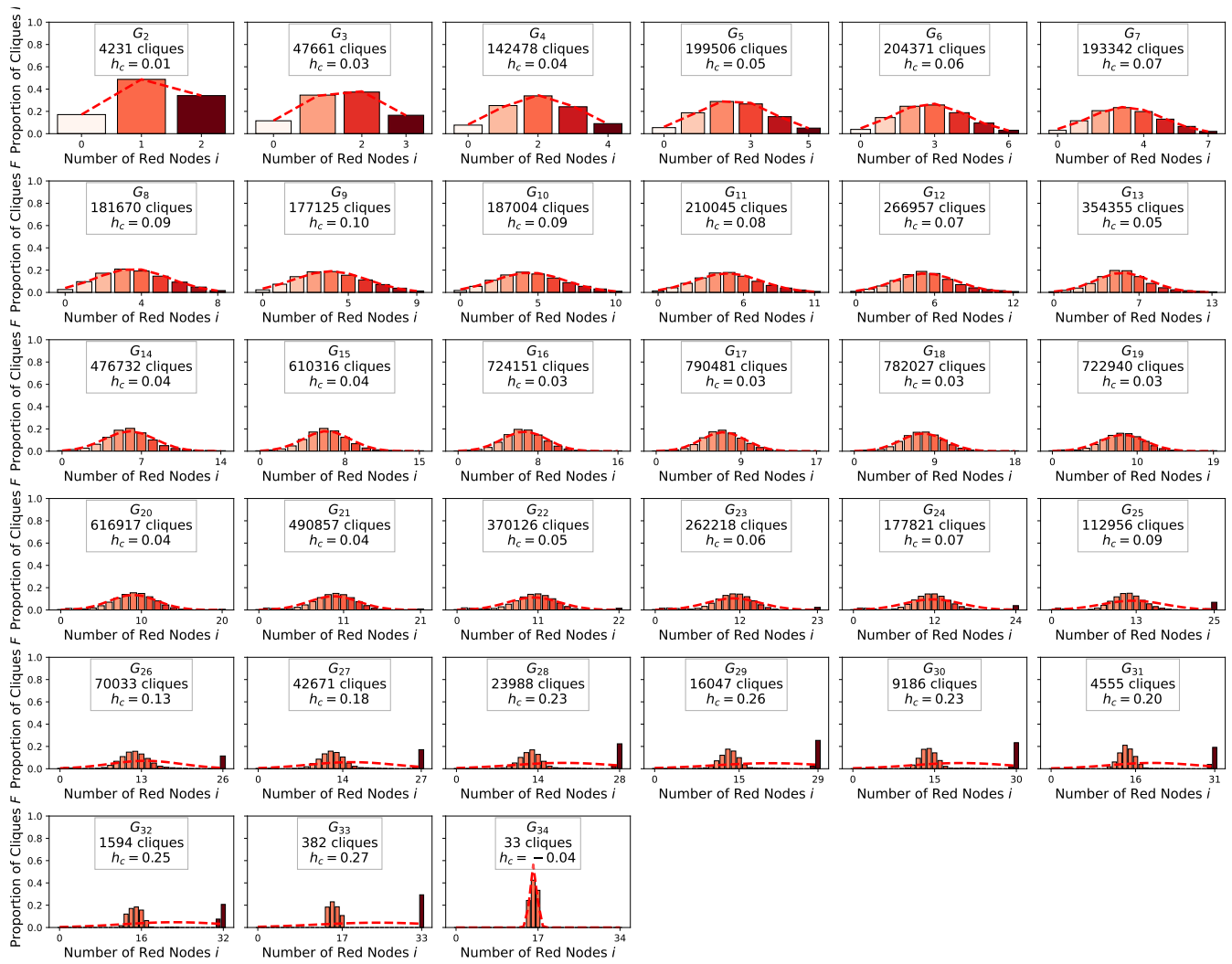


FIG. 15. Local homophily distributions for Duke University network, which consists of 9,895 nodes, with 56% red and 44% blue.

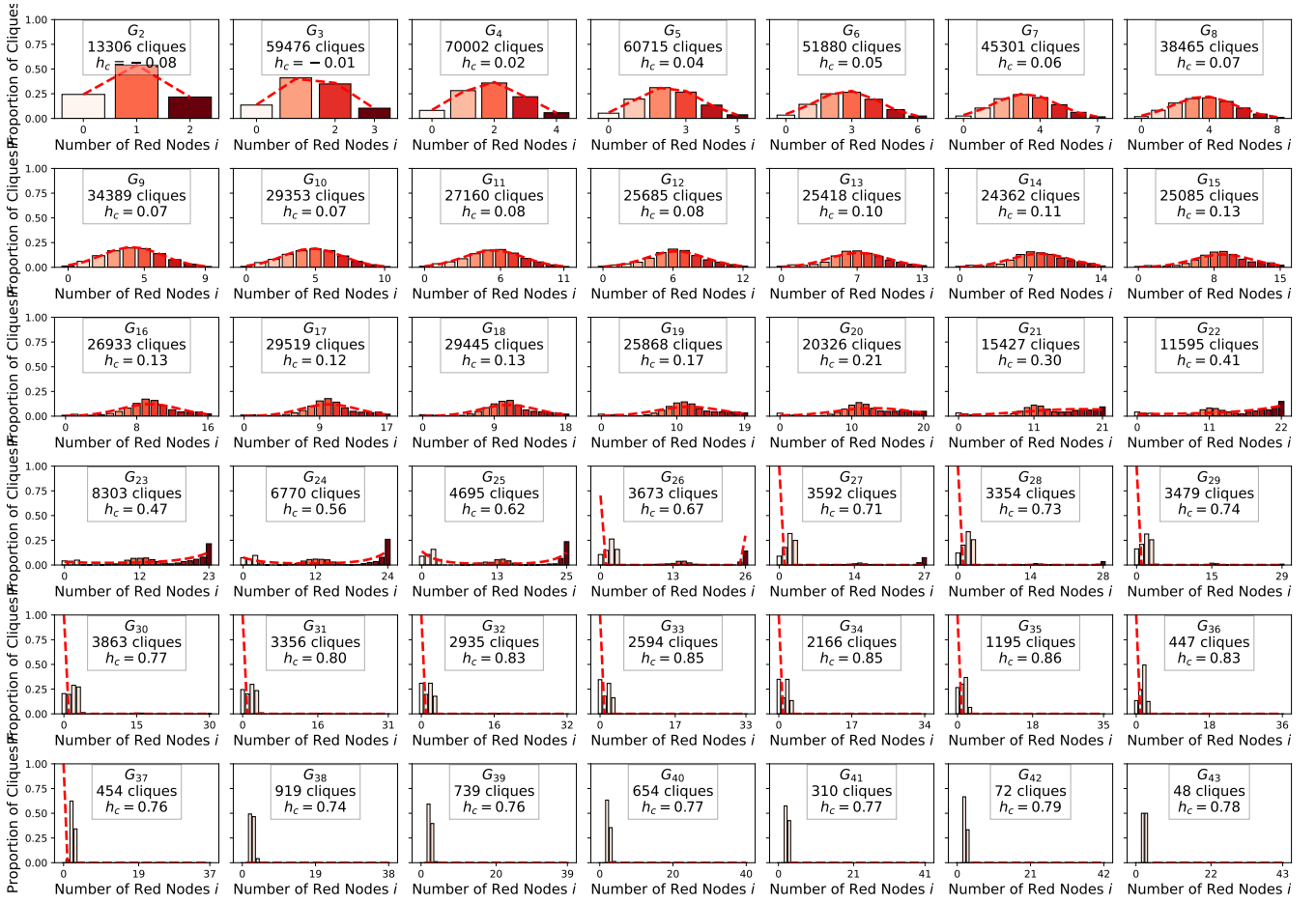


FIG. 16. Local homophily distributions for UCSD network, which consists of 14,984 nodes, with 50% red and 50% blue.

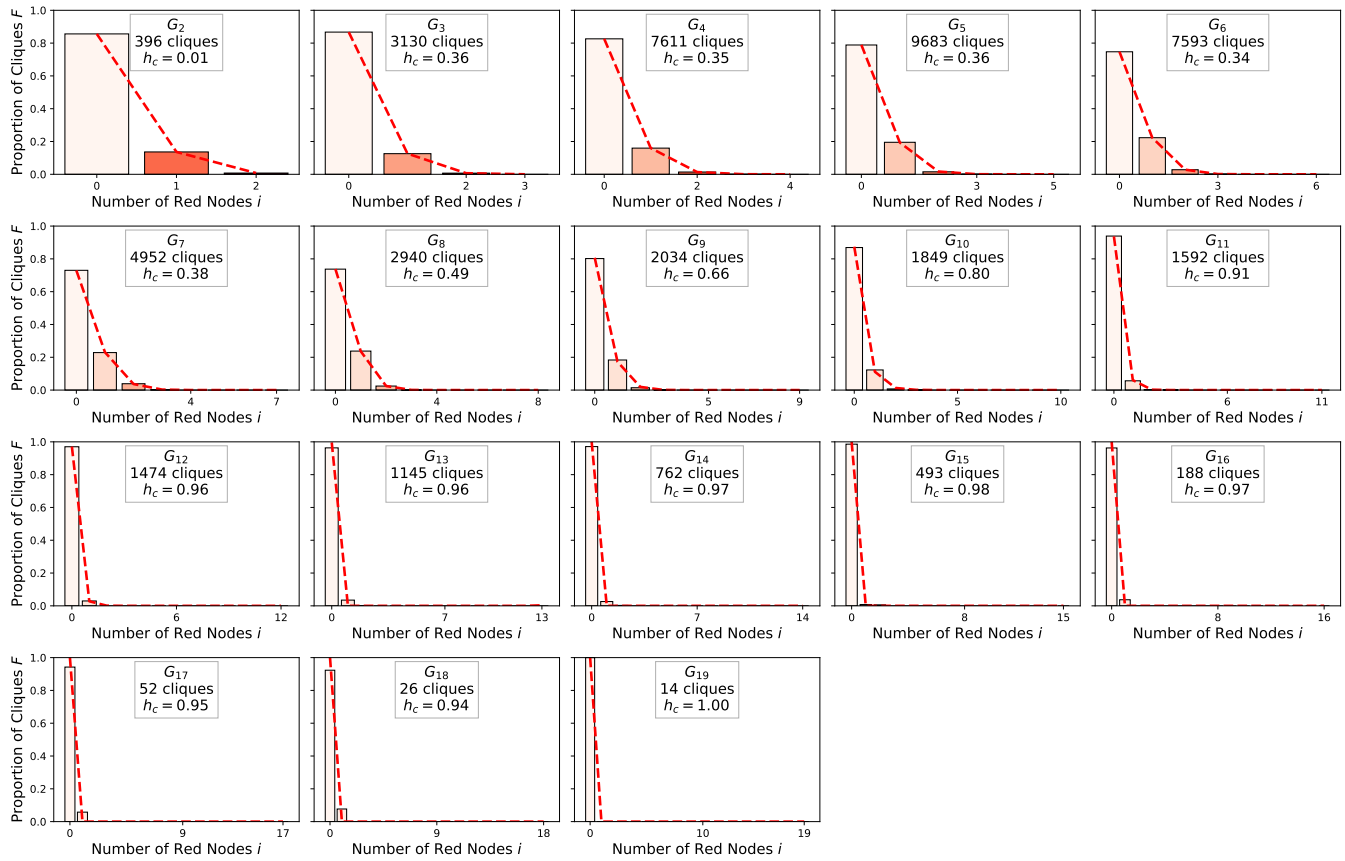


FIG. 17. Local homophily distributions for Simmons University network, which consists of 1,518 nodes, with 7% red and 93% blue.

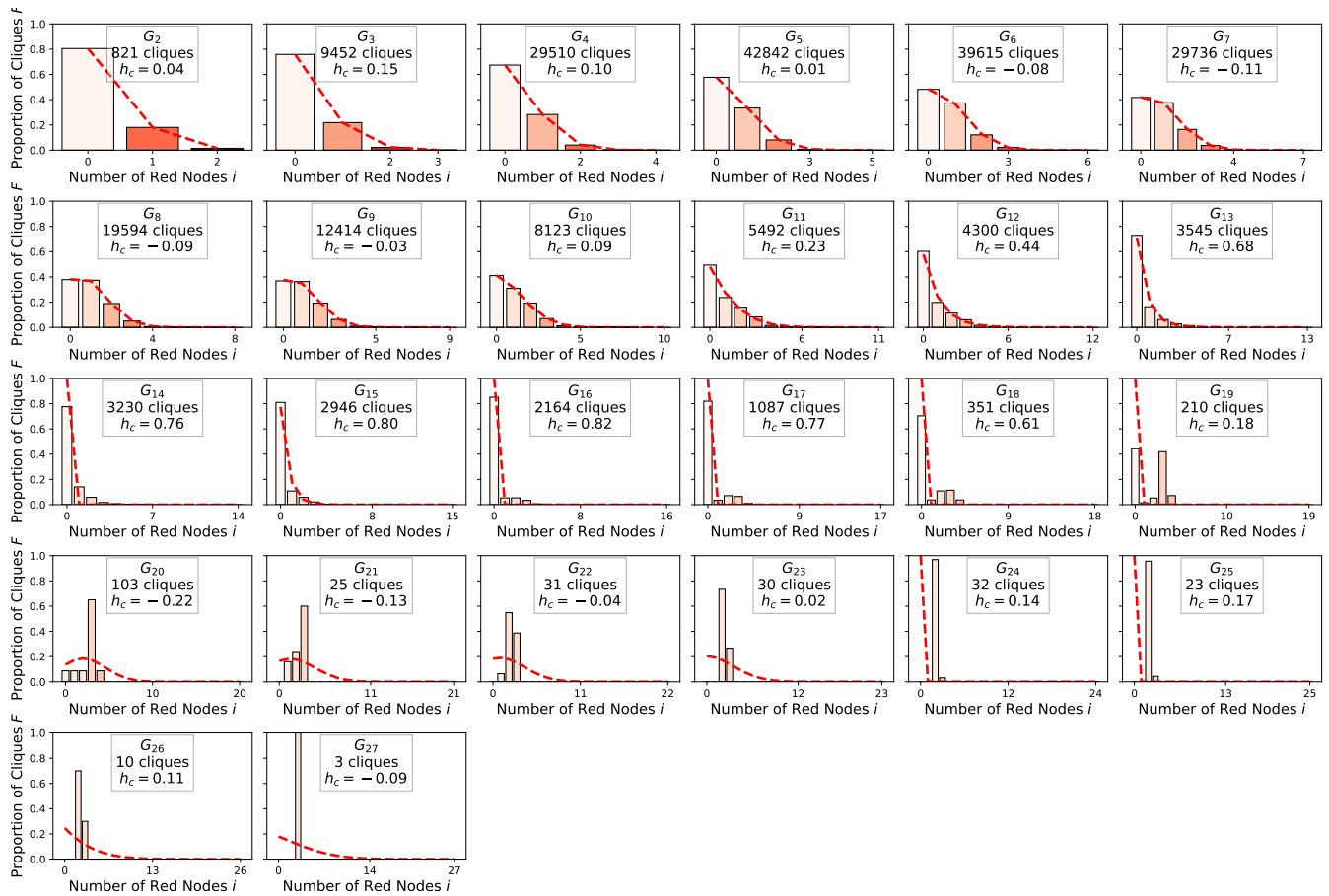


FIG. 18. Local homophily distributions for Wellesley College network, which consists of 2,970 nodes, with 11% red and 89% blue.

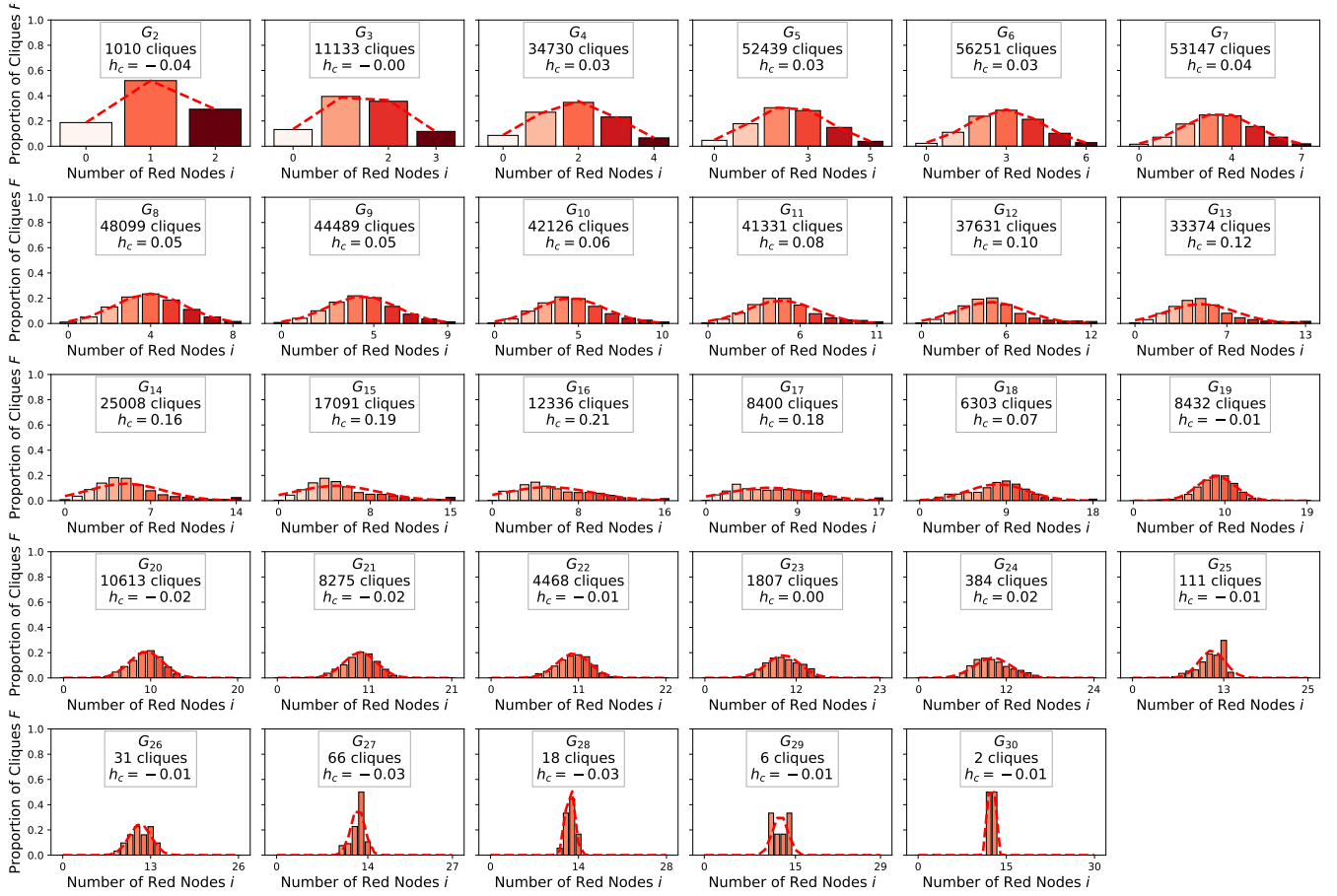


FIG. 19. Local homophily distributions for Wesleyan University network, which consists of 3,594 nodes, with 53% red and 47% blue.

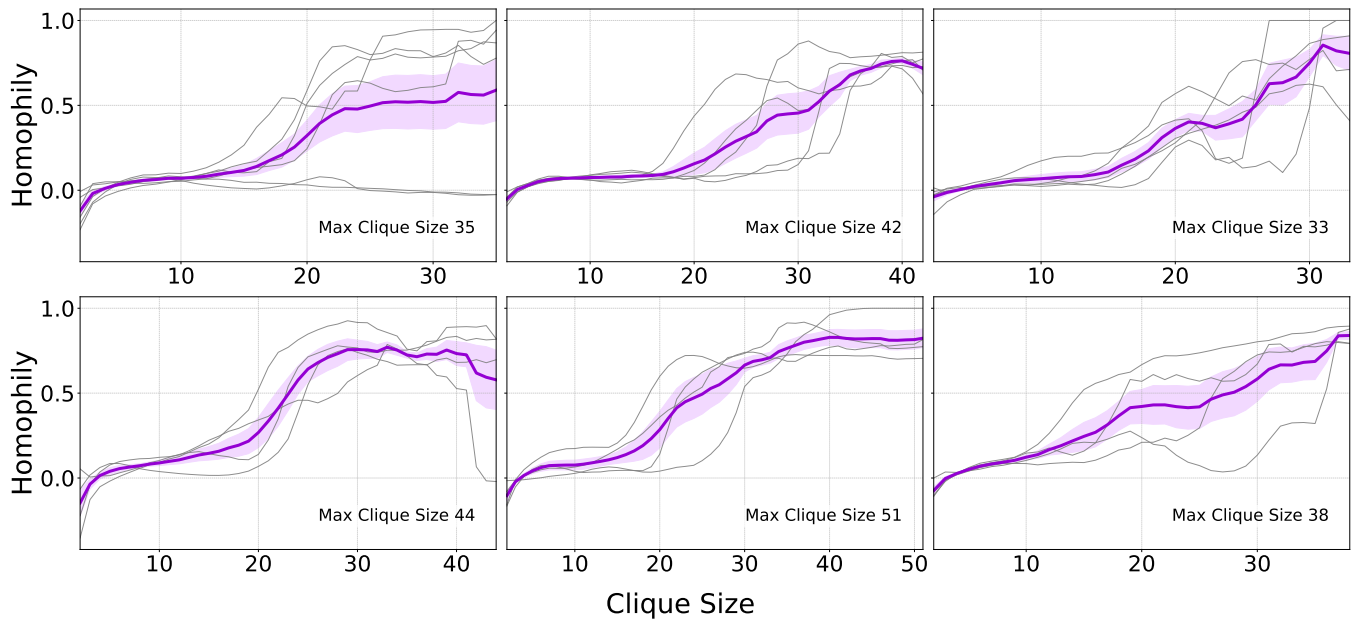


FIG. 20. Increasing pattern for homophily VS clique size in the Facebook friendship networks. Each panel displays individual curves in gray, representing networks of a specific maximal clique size, with the darker purple mean curve plotted on top. Shaded areas around the mean represent the standard error of the mean (SEM), providing insight into the variability of homophily within each length. The lengths with the highest number of curves are shown, with titles inside each panel indicating the length.

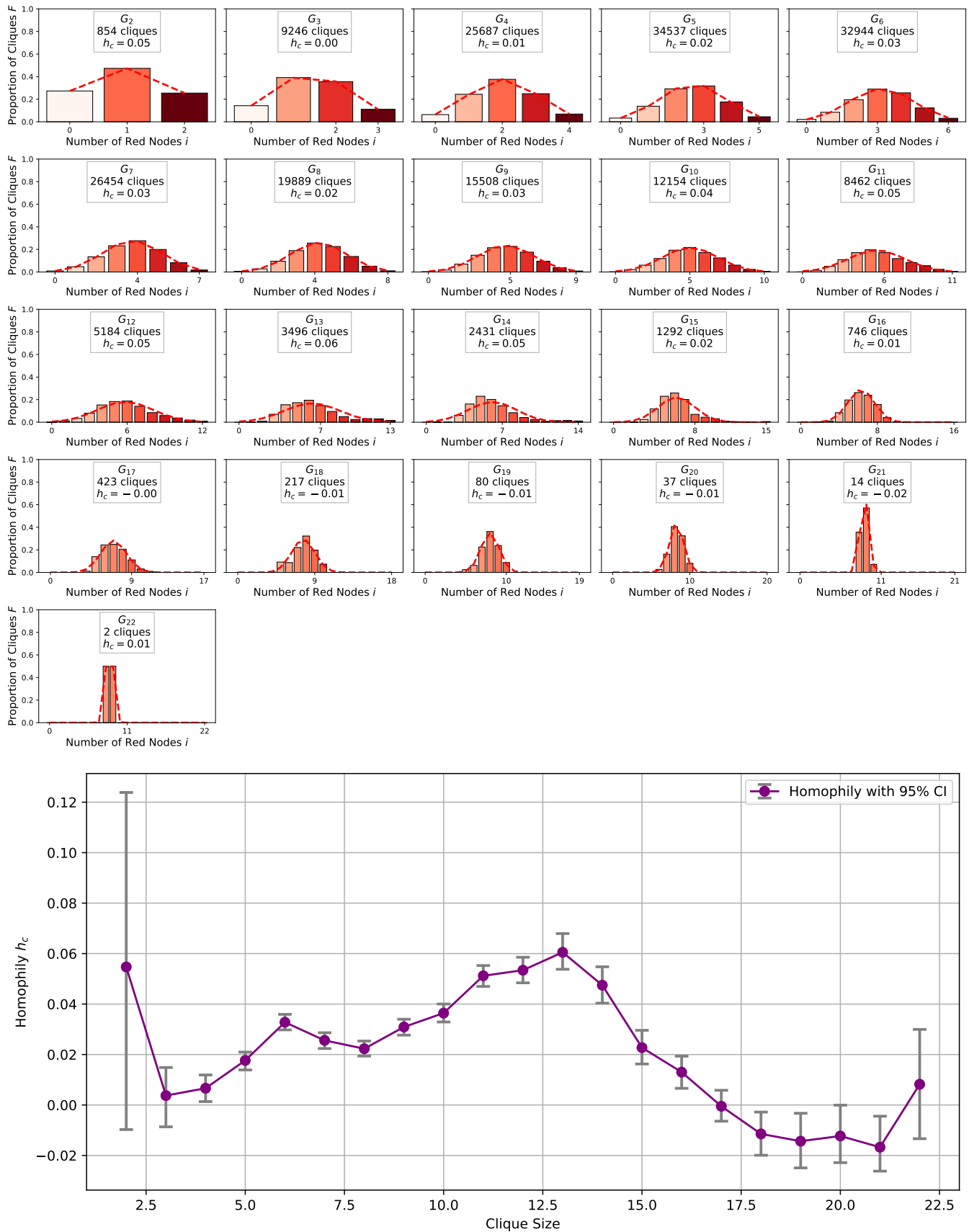


FIG. 21. Local homophily distributions for Oberlin College network, which consists of 2,920 nodes, with 49% red and 51% blue.

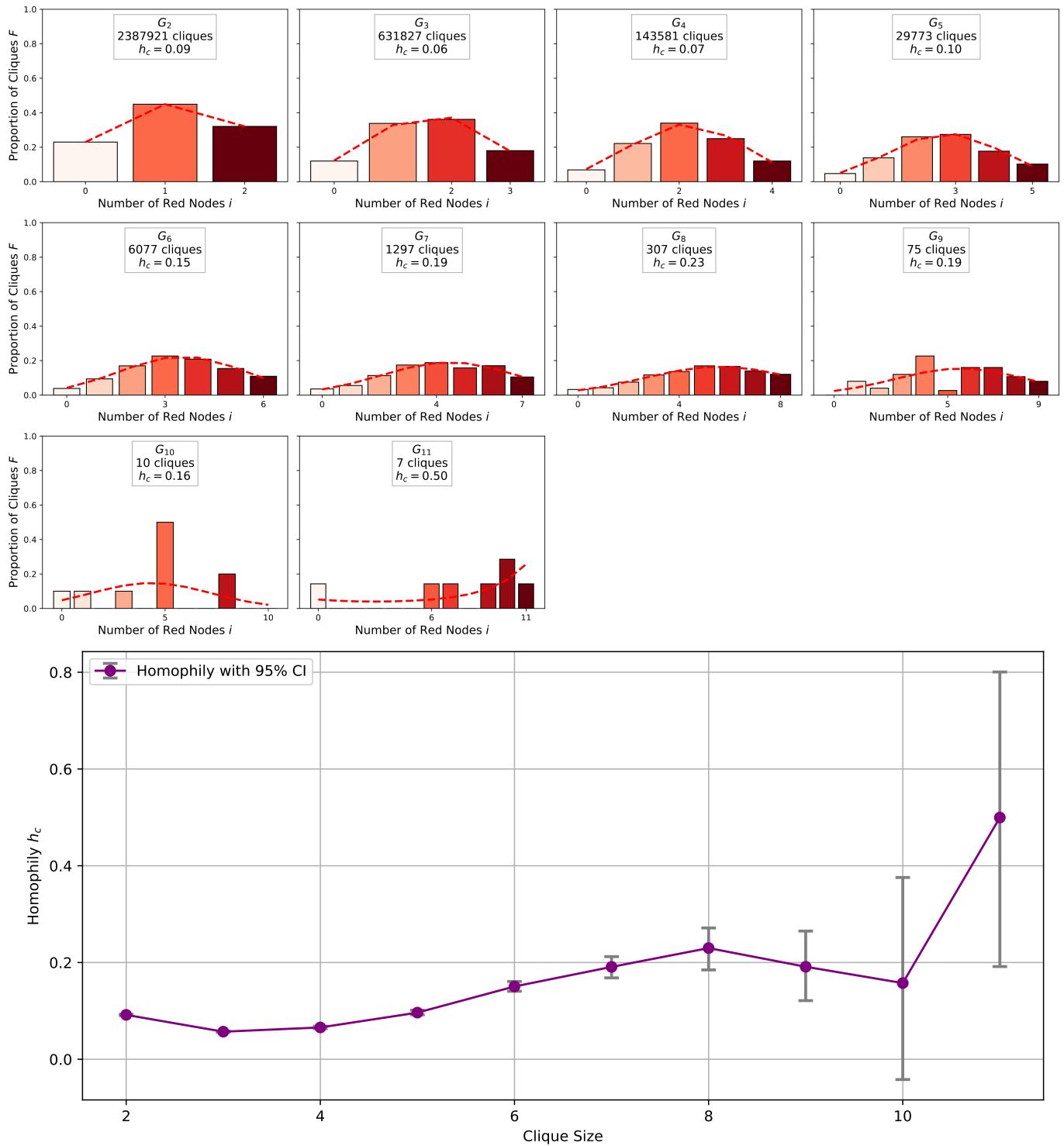


FIG. 22. Mobile Phone 2M nodes where 55.09% are red nodes and 44.91% are blue nodes. Homophily vs. Error bars represent 95% confidence intervals calculated using bootstrap resampling of cliques for each clique size.

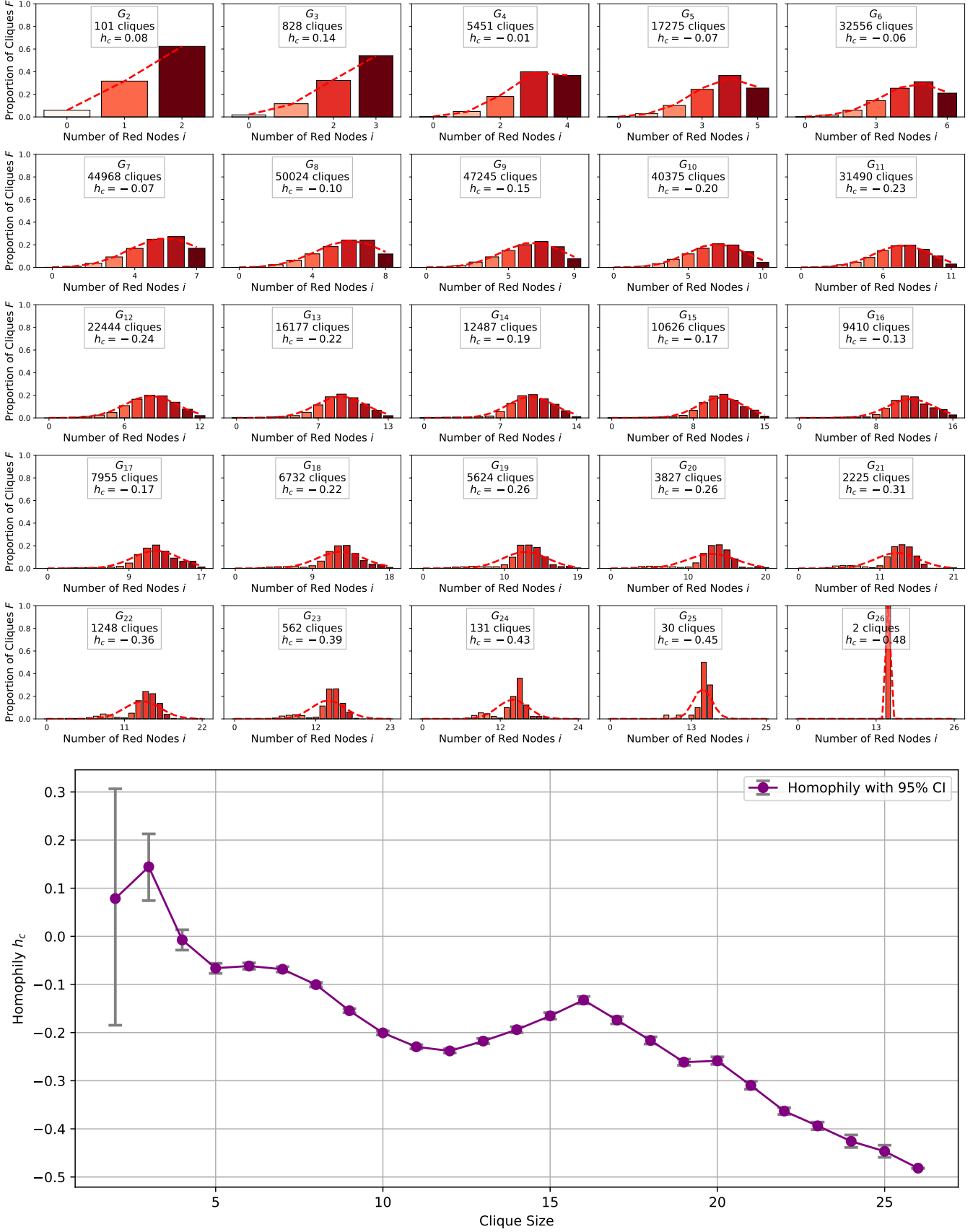


FIG. 23. Empirical and inferred distributions for the local homophily for the network of students in Copenhagen Study with 78.05% red nodes and 21.95% blue nodes.

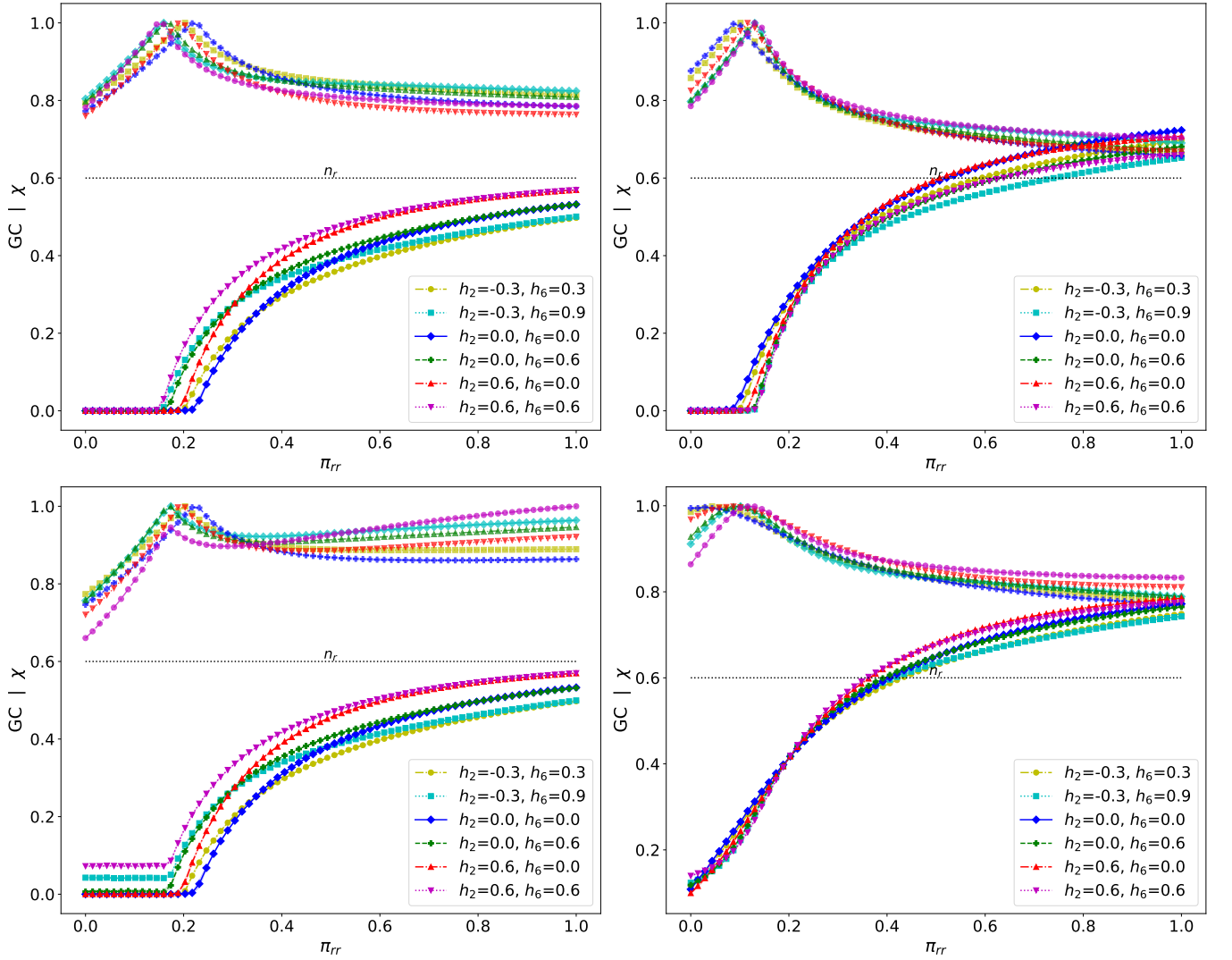


FIG. 24. Phase transition in the giant component of transmission networks where only red-red links are active with probability  $\pi_{rr}$ , with (top left) all blue-blue and blue-red links removed,  $\pi_{rb} = 0.0, \pi_{bb} = 0$ , (top right)  $\pi_{rb} = 0.2, \pi_{bb} = 0$ , (bottom left)  $\pi_{rb} = 0.0, \pi_{bb} = 0.2$ , (bottom right)  $\pi_{rb} = \pi_{bb} = 0.2$ . Lower curves depict the size of the giant component, while the top curves illustrate the peak susceptibility at the critical point. The average degree of the network is six. The phase transition is governed by the probability  $\pi_{rr}$  of red-red links remaining active. The higher the homophily values, especially strong (local) homophily, the lower the critical probability. When  $\pi_{rr} = 1$ , the transmission network only includes the red-red links, and these links contain a portion of the red nodes such that the larger the homophily, the larger this portion. In the extreme case of  $h = 1$ , where the network is segregated, the red-red links contain  $N_r$  red nodes. Note that at this extreme, the larger the weak (global) homophily, the larger the giant component. For smaller  $n_r$  values, the separations between the curves become more pronounced.

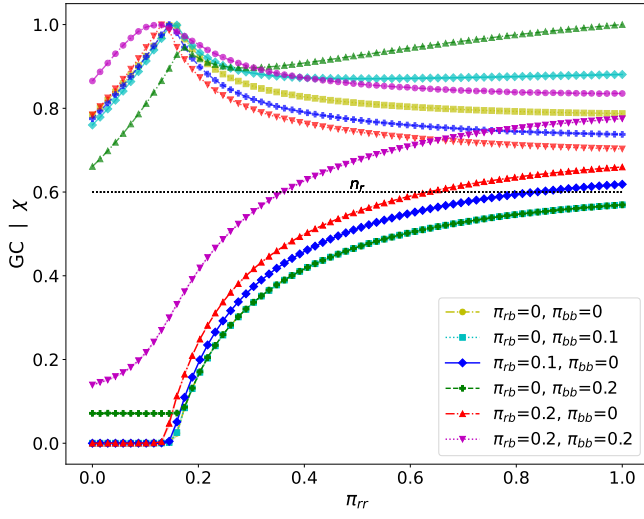


FIG. 25. How phase transition in a network with  $h_2 = h_6 = 0.3$  is different if we let the links leak (be active) with different probabilities. The average degree of the network is six. Lower curves depict the size of the giant component, while the top curves illustrate the susceptibility  $\chi$ , defined as the average size of the remaining components excluding the giant component.